



## BIROn - Birkbeck Institutional Research Online

Murphy, M. and Porcelli, D. and Pogge von Strandmann, Philip A.E. and Hirst, C. and Kutscher, L. and Katchinoff, J. and Morth, C. and Maximov, T. and Andersson, P. (2018) Tracing silicate weathering processes in the permafrost-dominated Lena River watershed using lithium isotopes. *Geochimica et Cosmochimica Acta* 245 , pp. 154-171. ISSN 0016-7037.

Downloaded from: <http://eprints.bbk.ac.uk/26026/>

*Usage Guidelines:*

Please refer to usage guidelines at <http://eprints.bbk.ac.uk/policies.html> or alternatively contact [lib-eprints@bbk.ac.uk](mailto:lib-eprints@bbk.ac.uk).

1 **Tracing silicate weathering processes in the permafrost-dominated Lena River watershed using**  
2 **lithium isotopes**

3  
4 Melissa J. Murphy<sup>\*a</sup>, Don Porcelli<sup>a</sup>, Philip A.E. Pogge von Strandmann<sup>b</sup>, Catherine A. Hirst<sup>c,d</sup>, Liselott  
5 Kutscher<sup>c,e</sup>, Joachim A. Katchinoff<sup>f</sup>, Carl-Magnus Mörrth<sup>e</sup>, Trofim Maximov<sup>g</sup>, Per S. Andersson<sup>c</sup>

6  
7 a Department of Earth Sciences, University of Oxford, South Parks Road, Oxford OX1 3AN, UK.

8 b London Geochemistry and Isotope Centre (LOGIC), Institute of Earth and Planetary Sciences,  
9 University College London and Birkbeck College, Gower Street, London, WC1E 6BT, UK.

10 c Department of Geosciences, Swedish Museum of Natural History, Box 50007, SE-104 05  
11 Stockholm, Sweden.

12 d Earth and Life Institute, Université catholique de Louvain, Croix du Sud, L7.05.10, B-1348  
13 Louvain-la-Neuve, Belgium

14 e Department of Geological Sciences, Stockholm University, SE-10691 Stockholm, Sweden.

15 f Department of Geology & Geophysics, Yale University, USA.

16 g Institute for Biological Problems of the Cryolithozone, Siberian Branch, Russian Academy of  
17 Science, Russia.

18  
19 \*Corresponding author: Now at: London Geochemistry and Isotope Centre (LOGIC), Institute of  
20 Earth and Planetary Sciences, University College London and Birkbeck College, Gower Street,  
21 London, WC1E 6BT, UK. Email address: [melissa.murphy@ucl.ac.uk](mailto:melissa.murphy@ucl.ac.uk)

22

23

24

25 **Abstract**

26           Increasing global temperatures are causing widespread changes in the Arctic, including the  
27 thawing of permafrost and the altering freshwater inputs and trace metal and carbon fluxes into  
28 the ocean and atmosphere. Strong seasonal changes in the permafrost active layer thickness can  
29 affect subsurface water flow-paths and water-rock interaction times, and hence weathering  
30 processes. Riverine lithium isotopes (reported as  $\delta^7\text{Li}$ ) are tracers of silicate weathering that are  
31 seemingly unaffected by biological uptake, redox, carbonate weathering and primary lithology. Here  
32 we use Li isotopes to examine silicate weathering processes in the catchment of one of the largest  
33 Russian Arctic rivers: the Lena River in eastern Siberia. The Lena River watershed is a large multi-  
34 lithological catchment, largely underlain by continuous permafrost. An extensive dataset of  
35 dissolved Li isotopic compositions of waters from the Lena River main channel, two main tributaries  
36 (the Aldan and Viliui Rivers) and a range of smaller sub-tributaries are presented from the post-  
37 spring flood/early-summer period at the onset of active layer development and enhanced water-  
38 rock interactions. The Lena River main channel (average  $\delta^7\text{Li}_{\text{diss}} \sim 19\text{‰}$ ) has a slightly lower isotopic  
39 composition than the mean global average of 23‰ (Huh et al., 1998a). The greatest range of [Li]  
40 and  $\delta^7\text{Li}_{\text{diss}}$  are observed in catchments draining the south-facing slopes of the Verkhoyansk  
41 Mountain Range. South-facing slopes in high-latitude, permafrost-dominated regions are typically  
42 characterised by increased summer insolation and high daytime temperatures, which contribute to  
43 more rapid thawing of snow cover, warmer soils, and repeated freeze/thaw cycles. The greater  
44 variability in Li characteristics in these rivers may then partly reflect the greater active layer thaw  
45 depth and hence greater infiltration of melt water typical of south-facing slopes in permafrost  
46 regions.

47           A similar magnitude of isotopic fractionation is observed between the contrasting low-lying  
48 regions of the Central Siberian Plateau (and catchments draining into the Viliui River), and  
49 catchments draining the mountainous regions of the Verkhoyansk Mountain Range into the Aldan  
50 River. This is in contrast to global rivers in non-permafrost terrains that drain high elevations or  
51 areas of rapid uplift, where high degrees of physical erosion promote dissolution of freshly exposed  
52 primary rock typically yields low  $\delta^7\text{Li}_{\text{diss}}$ , and low-lying regions exhibit high values resulting from  
53 greater water-rock interaction and formation of secondary mineral that fractionates Li isotopes.  
54 Overall, the range of Li concentrations and  $\delta^7\text{Li}_{\text{diss}}$  observed within the Lena River catchment show  
55 a similar range to compositions from global rivers located in temperate and tropical regions. This  
56 suggests that cryogenic weathering features specific to permafrost regions (such as the continual

57 exposure of fresh primary minerals due to seasonal freeze/thaw cycles, frost shattering and salt  
58 weathering), and indeed climate (temperature and runoff), are not a dominant control on  $\delta^7\text{Li}$   
59 variations. Despite vastly different climatic and weathering regimes, the same range of riverine  $\delta^7\text{Li}$   
60 values globally suggests that the same processes govern global Li geochemistry – that is, the balance  
61 between the dissolution of primary silicate minerals and the formation (or exchange with)  
62 secondary minerals. This has implications for the use of  $\delta^7\text{Li}$  as a palaeo-weathering tracer for  
63 interpreting changes in past weathering regimes.

64

## 65 **1. Introduction**

66 Permafrost thawing in high-latitude polar regions that is induced by climate warming influences  
67 mineral, elemental, nutrient and carbon fluxes (dissolved and particulate) into the ocean and  
68 atmosphere. Changes in the permafrost active layer thickness dictate subsurface water flowpaths,  
69 as well as water-rock interaction times and hence weathering processes, and this may impact future  
70 terrestrial biogeochemical cycles (Frey and McClelland, 2009). The evolution of long-term climate  
71 is influenced by the supply of cations from silicate weathering (providing alkalinity, which  
72 sequesters  $\text{CO}_2$  by carbonate precipitation in the oceans), as well as by delivering nutrients that  
73 facilitate organic carbon burial (Walker et al., 1981; Berner et al., 1983). To date, however,  
74 understanding the influence of climatic (e.g., temperature and runoff) and physical rock supply  
75 (e.g., sediment supply, physical erosion) controls on weathering are uncertain and highly debated  
76 (e.g., Raymo and Ruddiman, 1992; West et al., 2005; Hilley et al., 2010; Eiriksdottir et al., 2013).  
77 Changes in silicate weathering are in turn predicted to have significantly affected long- and short-  
78 term climate perturbations in the past (Raymo et al., 1988; Raymo and Ruddiman, 1992; Pogge von  
79 Strandmann et al., 2013).

80 Water-rock interactions, and hence silicate weathering, in cold-climate regions differ from  
81 those of warm and wet watersheds in temperate and tropical regions. The latter tend to be  
82 characterised by transport- or supply-limited regimes, where weathering rates are limited by the  
83 supply of fresh material, with long water-rock interaction times so that minerals are nearly  
84 completely altered before their removal and thick soils accumulate (West et al., 2005). In  
85 kinetically-limited weathering, the rate of chemical weathering is more limited relative to physical  
86 erosion. Soil production is limited because physical erosion removes weathered material more  
87 rapidly than it is produced, resulting in shorter water-rock interaction times (Stallard and Edmond,  
88 1983; West et al., 2005).

89 In high-latitude or alpine regions, low mean annual temperatures are expected to inhibit  
90 mineral reaction rates, resulting in incomplete weathering of silicate material (West et al., 2005).  
91 Nonetheless, it has been proposed that high rates of physical erosion from frost action and salt  
92 weathering, and enhanced primary rock dissolution by organic acids, can promote greater chemical  
93 weathering than might otherwise be expected in high-latitude regions dominated by temperature-  
94 controlled slow reaction rates (Gislason et al., 1996; Nezat et al., 2001; Huh, 2003).

95 Most weathering processes observed in weathering regimes in tropical and temperate  
96 climates are also prevalent in regions underlain by permafrost. However, the presence of  
97 permafrost further complicates water-rock interactions at high altitudes and polar regions.  
98 Permafrost underlies nearly a quarter of the northern hemisphere, and underlies approximately  
99 90% of the Lena River catchment, NE Siberia (Brown et al., 1997). Rivers in permafrost-dominated  
100 regions have very different hydrologic regimes to rivers in non-permafrost areas. In continuous  
101 permafrost-dominated catchments, perennially frozen soil/bed rock inhibits infiltration of surface  
102 water, thereby restricting subsurface water storage and limiting water-rock interactions. Rapid  
103 melting of winter precipitation (snow) accumulated within the catchment over ~8 to 9 months  
104 results in the high runoff spring freshet, which flows over the still frozen permafrost. In early spring,  
105 increasing air temperatures promote thawing of the near-surface and development of the 'active  
106 layer'. This enables water infiltration into the uppermost shallow (often organic-rich) thawed soil,  
107 and water is temporarily stored as ponded surface waters perched above the permafrost in low-  
108 lying wetlands and fens. Throughout the summer and early autumn before refreezing occurs, the  
109 active layer thaws to its maximum depth, potentially promoting exposure of more readily  
110 weathered rocks, deepening of flow paths and allowing greater water interaction with mineral-rich  
111 soil horizons (Woo, 2012). Unlike in tropical and temperate regions, the majority of hydrological  
112 processes (and hence silicate weathering) in permafrost-dominated terrains occurs within the  
113 seasonally thawed active layer (and regions of unfrozen talik) over the short thaw period. Rivers in  
114 watersheds with higher permafrost coverage tend to have lower subsurface storage capacity and  
115 thus a lower winter base flow and a higher summer peak flow compared to non-permafrost rivers  
116 (Woo, 2012; Yang et al., 2009).

117 In principle, climate warming could drive large annual changes in both the rate of silicate  
118 weathering and the weathering regime by contraction of the area underlain by continuous  
119 permafrost, increasing active layer thickness, and allowing greater suprapermafrost and talik  
120 groundwater flow (Frey and McClelland, 2009). This could affect the biogeochemical cycles of many

121 elements and the supply of micronutrients to northern oceans. It could also impact the Earth's  
122 climate feedback cycles through the release of carbon trapped within permafrost into the  
123 atmosphere and oceans. Since the response of weathering processes to permafrost thawing is not  
124 well understood (Pokrovsky et al., 2005; Frey et al., 2007; Frey and McClelland, 2009; Keller et al.,  
125 2010), it is unknown whether carbon removal via silicate weathering or carbon release from  
126 permafrost thawing will have the greatest effect on the carbon budget. Constraining the processes  
127 that govern silicate weathering in high-latitude, permafrost dominated regions is therefore critical  
128 for quantifying the global carbon cycle over modern and geological timescales.

129 To date, it has proven difficult to constrain weathering processes at any scale, particularly in  
130 permafrost-dominated regions, because most tracers that are used are affected by multiple  
131 processes (e.g. biology, lithology, redox, etc.). Riverine lithium isotope ratios ( $^{7}\text{Li}/^{6}\text{Li}$ , reported as  
132  $\delta^{7}\text{Li}$ , that is the ‰ deviation from the  $^{7}\text{Li}/^{6}\text{Li}$  ratio of the L-SVEC standard) trace silicate weathering  
133 processes at scales ranging from soils and small monolithological catchments to significant global  
134 river watersheds that integrate large areas of variable lithology and often several climatic regions.  
135 Lithium isotopes are not fractionated in the environment by biological processes (Lemarchand et  
136 al., 2007; Pogge von Strandmann et al., 2016). Also, Li is orders of magnitude more concentrated in  
137 silicates over carbonates, so that even in carbonate catchments, Li isotopes are dominated by  
138 silicate weathering (Kisakúrek et al., 2005; Millot et al., 2010). River  $\delta^{7}\text{Li}$  values are controlled by  
139 what has been described as “silicate weathering congruency” (Misra and Froelich, 2012; Pogge von  
140 Strandmann and Henderson, 2015; Vigier and Godd ris, 2015; Pogge von Strandmann et al., 2016;  
141 2017). This is defined as the ratio of primary mineral dissolution (releasing largely unfractionated Li  
142 with crustal  $\delta^{7}\text{Li} \sim 0$  to 5‰) to secondary mineral formation (which preferentially incorporate  $^{6}\text{Li}$ ,  
143 increasing the  $\delta^{7}\text{Li}$  composition of Li remaining in solution; Pistiner and Henderson, 2003; Vigier et  
144 al., 2008; Wimpenny et al., 2010a). High riverine  $\delta^{7}\text{Li}$  values have been interpreted as reflecting less  
145 complete weathering, greater secondary mineral formation and thus greater ‘weathering intensity’  
146 (i.e., the ratio of chemical to physical denudation; Bouchez et al., 2013; Dellinger et al., 2015). There  
147 have been a number of large global rivers in tropical and temperate environments where the  
148 behaviour of Li isotopes has been studied: e.g., the Amazon River (Chan et al., 1992; Huh et al.,  
149 1998a; Dellinger et al., 2014, 2015); the Orinoco River (Huh et al., 1998a; Huh et al., 2001); rivers in  
150 the high Himalayas and the Ganges-Brahmaputra (Huh et al., 1998a; Kisakúrek et al., 2005; Bagard  
151 et al., 2015; Manaka et al., 2017; Pogge von Strandmann et al., 2017) the Changjiang (Yangtze)  
152 River (Huh et al., 1998a; Liu et al., 2011; Wang et al., 2015); the Mississippi River (Chan et al., 1992;

153 Huh et al., 1998a) and the Congo River (Henchiri et al., 2016). However, there are fewer studies of  
154 rivers draining cold climate regions. Whilst some data from Siberia exist, the sampling sites are  
155 limited to a handful of locations from the major tributaries and river mouths (Huh et al., 1998a). The  
156 only comparable studies of high-latitude polar regions are the Mackenzie River basin (Millot et al.,  
157 2010) and the comparatively short rivers of Iceland (Pogge von Strandmann et al., 2006; Vigier et  
158 al., 2009; Pogge von Strandmann et al., 2016), Greenland (Wimpenny et al., 2010b), the McMurdo  
159 Dry Valleys in Antarctica (Witherow et al., 2010), and Svalbard (Hindshaw et al., 2018).

160 In this study, Li isotopic compositions were measured in over 70 river samples and 11  
161 suspended sediments across the catchment of the vast and relatively unstudied Lena River in  
162 eastern Siberia. The multi-lithological catchment spans a latitudinal and climate gradient from 60°  
163 to 68° N and is largely underlain by continuous permafrost. The effects of secondary mineralogy,  
164 climate, topography and presence of permafrost on silicate weathering are investigated. This study  
165 vastly increases the amount of Li isotope data from high latitudes, which has been limited partly  
166 due to difficulties in logistics and gaining access.

167

## 168 **2. Background**

### 169 **2.1 Study Area**

170 The Lena River basin is located in Yakutia in eastern Siberia (Fig. 1). The Lena River is one of  
171 the largest Russian Arctic rivers, draining a watershed area of  $2.46 \times 10^6$  km<sup>2</sup>. The river flows  
172 northwards from 53°N near Lake Baikal to 71°N and enters the Arctic Ocean in the Laptev Sea. The  
173 headwaters originate in the discontinuous and patchy mountain permafrost of the Baikal, Stanovoi  
174 and Dzhugdzhur mountains. Northward from 60°N latitude, the Lena River watershed is underlain  
175 by variable thicknesses of continuous permafrost ranging from 50 meters to over 1500 m (Brown et  
176 al., 1997; Chevychelov and Bosikov, 2010). The seasonally thawed active layer varies in thickness  
177 throughout the catchment from a few centimetres to several meters (Huh et al., 1998c). The Lena  
178 River contributes approximately 15% of the total freshwater input into the Arctic Ocean, of which  
179 ~85% is provided during the spring flood and summer months (May – September; Ye et al., 2003).  
180 The geology of eastern Siberia has been described in detail by Gordeev and Sidorov, (1993), Huh et  
181 al. (1998b, 1998c), and Huh and Edmond, (1999). Briefly, the Central Siberian Plateau (CSP; see Fig.  
182 1) is underlain by Proterozoic crystalline and metamorphic basement of the stable Siberian Platform,  
183 which outcrop to the south in the mountainous Trans-Baikal region where the headwaters of the  
184 Lena River form, and to the east in the Archean Aldan-Stanovoy shield mountains which are drained

185 by rivers in the Lena-Amginsky inter-river area (LAIRA). The CSP is typified by gentle topography and  
186 extensive flood plains, with thick sedimentary cover composed of Precambrian to Quaternary  
187 marine carbonates and evaporites, along with terrigenous sandstone, shale, red beds, and coal  
188 beds. The Verkhoyansk Mountain Range forms a topographic high to the east, and is composed of  
189 folded and metamorphosed rocks and uplifted detrital sediments. It is not actively undergoing  
190 tectonic uplift.

191 The climate of the watershed is continental, characterised by long cold winters and short,  
192 hot summers, with temperatures ranging from  $-50\text{ }^{\circ}\text{C}$  to  $+35\text{ }^{\circ}\text{C}$ . The mean annual air temperature  
193 (MAAT) ranges from  $-6$  to  $-15\text{ }^{\circ}\text{C}$  across the region and decreases with increasing latitude (Fedorov  
194 et al., 2014). The mean annual precipitation (MAP) is typically low, ranging from 200 to 500 mm/yr  
195 (Chevychelov and Bosikov, 2010). The drainage area is mainly composed of boreal taiga forest of  
196 larch and salix in the southern parts of the basin, with exposed rock outcrops, small shrubs, moss  
197 and lichen in the tundra regions of the northern part of the basin (Gordeev and Sidorov, 1993).

198

### 199 **3. Analytical methods**

#### 200 **3.1 Field sampling**

201 The samples and methods are described in detail by Hirst et al. (2017) and Kutscher et al. (2017).  
202 Briefly, sampling occurred over two field campaigns (summer of July 2012 and late spring/early  
203 summer of June 2013) when the active layer is thickest and so suprapermafrost groundwater flow  
204 is deepest. Sampling dates, locations and descriptions are given in Fig. 1 and Table S1. In the field,  
205 surface water samples were collected in acid-washed 10 L low density polyethylene (LDPE) bottles  
206 by grab sampling from the upstream side of the ship or small motorised boat, or by wading out into  
207 river channels. Samples were filtered within a few hours using a polycarbonate Geotech<sup>®</sup> filter  
208 holder and  $0.22\text{ }\mu\text{m}$  nitrocellulose filters (Millipore<sup>®</sup>) prewashed with 5% acetic acid and ultrapure  
209 Milli-Q water. At each sampling locality, pH, temperature and electrical conductivity were measured  
210 *in-situ* using a multi-meter (YSI 556 multiprobe system) with analytical accuracies of  $\pm 0.03$  pH units,  
211  $\pm 0.1\text{ }^{\circ}\text{C}$ , and  $\pm 1\text{ }\mu\text{S/cm}$ .

212 The rivers for this study have been geographically grouped according to Kutscher et al.  
213 (2017): (i) the Lena River main channel; (ii) the low-lying Central Siberian Plateau (CSP) tributaries;  
214 (iii) the main channel of the major Viliui River tributary that is sourced from that region; (iv) the  
215 mountainous tributaries draining the Verkhoyansk Mountain Range (VMR); (v) the main channel of



216 the major Aldan River tributary; and (vi) tributaries draining the Lena-Amginsky inter-river area  
217 (LAIRA).

218

### 219 **3.2 Major cation and trace element analyses**

220 Major cations were measured by Inductively Coupled Plasma Optical Emission Spectroscopy (ICP-  
221 OES Thermo Icap 6500 Duo) at the Department of Geological Sciences, Stockholm University. For  
222 details, see Sun et al. (2018). For the majority of samples, Li concentrations were analysed using an  
223 Element 2 sector-field Inductively-Coupled-Plasma Mass Spectrometer (ICP-MS) at the University of  
224 Oxford. For Li analyses, standard addition calibration curves were prepared by doping a given  
225 sample with a multi-elemental standard solution (Alfa Aesar®) to account for matrix effects. Both  
226 standard and water samples were doped with 1 ng/g of rhenium internal standard to correct for  
227 instrumental drift. Accuracy was assessed by analysing IAPSO seawater and the international river  
228 reference standard SLRS-5, and by measuring samples in duplicate, and external analytical  
229 uncertainties were better than 5%. For a handful of samples with Li concentrations below the limit  
230 of detection on the Element 2 (<60 nM Li, see Table 1), concentrations were estimated by intensity  
231 matching against a known concentration of L-SVEC on the MC-ICP-MS (see below), with  
232 uncertainties estimated to be  $\pm 10\%$ .

233

### 234 **3.3 Li isotope measurements**

235 For Li isotope analysis of the waters, a sufficient volume of each sample was evaporated to yield 10-  
236 20 ng Li, and refluxed 1-2 times with concentrated HNO<sub>3</sub> to break down organics prior to separation.  
237 This stage is necessary in these organic-rich samples, and resulted in an improvement of internal  
238 precision on the measurements by *ca.* 50%. For the suspended sediments, filters were digested  
239 using protocols outlined by Hirst et al. (2017). Evaporated water samples and aliquots of the filter  
240 digests were dissolved in 0.2 M HCl and passed through a two-stage cation exchange  
241 chromatography procedure (BioRad® AG50W-X12), using dilute HCl as an eluent (Pogge von  
242 Strandmann et al., 2011; Pogge von Strandmann and Henderson, 2015). In order to confirm that  
243 quantitative Li yields on the column were achieved and no significant fractionation occurred on the  
244 column, aliquots before and after the main elution were analysed. Blanks for the total chemical  
245 procedure were less than 5 pg Li, which is negligible relative to the 10–20 ng of Li analysed in each  
246 sample.

247 Lithium isotope compositions were determined on a Nu Plasma HR-MC-ICP-MS at the  
248 Department of Earth Sciences, University of Oxford, in dry plasma mode using a Cetac Aridus-II  
249 desolvating system. Corrections for instrumental mass bias were made using sample-standard  
250 bracketing. Data are reported in  $\delta^7\text{Li}$  notation, the permil deviation of the measured  $^7\text{Li}/^6\text{Li}$  ratio  
251 from the L-SVEC standard (NIST SRM 8545; Flesch et al., 1973), where  $\delta^7\text{Li} = [(^7\text{Li}/^6\text{Li}_{\text{sample}}) / (^7\text{Li}/^6\text{Li}_{\text{L-SVEC}}) - 1] \times 1000$ . Each sample was analysed in triplicate during the course of each run. Individual  
252 errors are the two standard deviation around the mean of at least two, but typically three, replicate  
253 measurements. The external reproducibility was determined by repeat measurements of an internal  
254 seawater standard processed through the full chemical procedure, which yielded  $\delta^7\text{Li} = 31.3 \pm 0.7\text{‰}$   
255 (2sd;  $n = 20$ ). Two rock standards were also run, granite JG-2 ( $\delta^7\text{Li} = 0.4 \pm 0.2\text{‰}$ ,  $n=3$ ) and Wyoming  
256 oil shale SGR-1b ( $\delta^7\text{Li} = 3.6 \pm 0.4\text{‰}$ ,  $n=3$ ), and the results are within uncertainty of other published  
257 values (Pogge von Strandmann et al., 2017 and references therein). Replicates of samples processed  
258 in duplicate ( $n = 9$  waters, 3 sediments) in different analytical sessions are indistinguishable from  
259 one another within analytical error, with the exception of LR2012-37, which shows slightly greater  
260 variability (1.5‰; Table 1). Duplicates are plotted as the average of the two measurements.  
261

262

#### 263 **4. Results**

264 Sample location and field parameter data (from Hirst et al. 2017; Kutscher et al. 2017), dissolved  
265 [Na] and [Li] (where square brackets denote concentrations),  $\delta^7\text{Li}_{\text{diss}}$  and suspended sediment  
266  $\delta^7\text{Li}_{\text{susp}}$  are given in Table 1. Other major elemental data are presented in Sun et al. (2018). Lithium  
267 concentrations range from 12 to 1520 nM. This range is similar to that observed from long-term  
268 seasonal monitoring of the Lena River at Zhigansk (Fig. 1, [Li] = 115 to 628 nM; Holmes et al., 2018).  
269 Dissolved  $\delta^7\text{Li}$  values range between +7.1 and +41.9‰ (Fig. 2). Despite the large range of values, the  
270 average  $\delta^7\text{Li}_{\text{diss}}$  for the geographical regions vary within only a few permil. Average [Li] and  $\delta^7\text{Li}_{\text{diss}}$   
271 compositions are presented as box-and whisker plots in Supplementary Fig. 1. Lithium  
272 concentrations within the Lena River main channel (average ~134 nM) are lower than the global  
273 mean of 215 nM, and are similar to shield-draining rivers elsewhere (Huh et al., 1998a). The Viliui  
274 River as well as the tributaries of the CSP, LAIRA and VMR have higher average [Li] (232 to 338 nM)  
275 when compared to the Lena River main channel and Aldan River. The greatest ranges in both [Li]  
276 and  $\delta^7\text{Li}$  are observed in rivers draining the Verkhoyansk Mountain Range (VMR), and especially in  
277 catchments that predominantly have a south-facing aspect (See Fig. 1 and Table 1). Overall, the data  
278 presented here are comparable with the more limited previously published data in the Lena River

279 catchment ( $[Li] = 40$  to  $3350$  nM;  $\delta^7Li = 19.0$  to  $29.9\text{‰}$ ; Huh et al., 1998a). The furthest downstream  
280 sample from this study (LR2013-45,  $[Li] = 192$  nM,  $\delta^7Li = 21.3\text{‰}$ ) is indistinguishable to sample UL607  
281 from the Lena River outflow  $\sim 500$  km at Kusur measured previously ( $[Li] = 220$  nM,  $\delta^7Li = 21.5\text{‰}$ ;  
282 Huh et al., 1998a). Both samples LR2013-45 and UL607 were collected during the early summer  
283 months (in June 2013 and July 1995, respectively).

284 Using published monthly discharge and  $[Li]$  data from R-ArcticNet ([http://www.r-](http://www.r-arcticnet.sr.unh.edu/v4.0/index.html)  
285 [arcticnet.sr.unh.edu/v4.0/index.html](http://www.r-arcticnet.sr.unh.edu/v4.0/index.html)), ArcticRIMS (<http://rims.unh.edu/data.shtml>) and the Arctic  
286 Great Rivers Observatory (<http://arctic.greaterivers.org/data.html>), an annual discharge-weighted  
287 Li flux into the Arctic Ocean of  $1.29 \times 10^8$  mol/yr can be calculated. Using a  $[Li] = 192$  nM of our  
288 northernmost sample (LR2013-45) and the average annual discharge, we obtain an annual flux of  
289  $1.03 \times 10^8$  mol/yr, which is comparable to the estimate of  $1.18 \times 10^8$  mol/yr by Huh et al. (1998a). This  
290 accounts for approximately 1% of the global riverine Li flux into the ocean.

291 The Li isotopic composition of the Lena River main channel is relatively uniform throughout  
292 the catchment ( $\sim 19 \pm 2\text{‰}$ ;  $1\sigma$ ), and is several permil lower than the global riverine mean of  $\sim 23\text{‰}$   
293 (Huh et al., 1998a), with the exception of one atypical sample with high  $[Li]$  and  $\delta^7Li$  (LR2013-41;  
294  $\delta^7Li = 29.0\text{‰}$ ,  $396$  nM). The ranges of  $\delta^7Li$  and  $[Li]$  measured in this study are similar to those of data  
295 from other large global rivers systems elsewhere (e.g., the Mackenzie River, Millot et al., 2010; the  
296 Ganges-Brahmaputra, Kısakürek et al., 2005, Bagard et al., 2015, Pogge von Strandmann et al., 2017;  
297 and the Amazon, Dellinger et al., 2015).

298 The rivers in the Lena catchment show a broad negative trend between  $\delta^7Li_{diss}$  and  $[Li]$ ,  
299 although the lack of a simple relationship between  $\delta^7Li$  and Li concentration for the Lena River main  
300 channel and the main catchment regions (Fig. 2) indicates that there are a range of processes  
301 controlling the Li concentrations and isotope variations. In particular, the data cannot be adequately  
302 explained by simple mixing between two endmembers with different isotopic compositions and  
303 weathering regimes, as has been inferred for the Mackenzie River Basin (Millot et al., 2010) and the  
304 Congo River (Henchiri et al., 2016). This is not unexpected in such a large complex, multi-lithological  
305 drainage region.

306 Four sets of samples were collected from the same locations in both the July 2012 and June  
307 2013 field campaigns (Table 1; LR2012-23/LR2013-77 and LR2012-24/LR2013-76 from a tributary  
308 draining the VMR; LR2012-03/LR2013-78 from the main channel of the Lena River; and LR2012-  
309 22/LR2013-38 from the Aldan River). With the exception of the LR2012-24/LR2013-76 pair of  
310 samples, which had similar  $[Li]$ , the concentrations of samples collected in 2013 were almost double

311 those of their 2012 counterparts. In all instances, however, the  $\delta^7\text{Li}$  values of the samples from the  
312 same locations sampled during both campaigns were within 1-2‰ of one another. This might  
313 suggest that despite presumed increases in the thickness of the active layer during the warmer  
314 months, there is only limited  $\delta^7\text{Li}$  variation.

315 The suspended sediments have a narrow  $\delta^7\text{Li}_{\text{susp}}$  range from +0.4 to +5.1‰ (Supplementary  
316 Fig. 2), which broadly overlaps with average continental silicate rock values (UCC,  $\sim 0.6 \pm 0.6\text{‰}$ ,  
317 Teng et al., 2004; Sauzéat et al., 2015; and basalts  $\sim 3$  to  $5\text{‰}$ , Elliott et al., 2006, Tomascak et al.,  
318 2008). The suspended sediments are isotopically heavier than the global mean suspended sediment  
319 Li isotopic composition for large global rivers of  $-1.5 \pm 1\text{‰}$  ( $1\sigma$ ; Dellinger et al., 2014) but comparable  
320 to  $\delta^7\text{Li}_{\text{susp}}$  values for other rivers (e.g., the Mackenzie River, Millot et al. 2010; the Ganges-  
321 Brahmaputra; Kısakúrek et al. 2005, Bagard et al. 2015, Pogge von Strandmann et al. 2017; the  
322 Dongqu, Weynell et al., 2017); and the Amazon, Dellinger et al., 2014). Variations in  $\delta^7\text{Li}$  have been  
323 reported for suspended sediments related to variations in Si/Al (a proxy for grain size) in depth  
324 profiles in the Amazon, Mackenzie and Ganges-Brahmaputra Rivers that are the result mineral  
325 sorting within the water column (Bouchez et al. 2011, Dellinger et al. 2014, Dellinger et al. 2017).  
326 However, only suspended sediments from near-surface waters have been collected in this study,  
327 and the use of HF in the filter dissolution protocol in these samples precludes the use of Si/Al as a  
328 proxy for grain size.

329 The variation in isotopic offset between  $\delta^7\text{Li}_{\text{susp}}$  and  $\delta^7\text{Li}_{\text{diss}}$  for the different geographical  
330 regions within the Lena River watershed are shown in Supplementary Fig. 3. The range of isotopic  
331 fractionation factors ( $\Delta^7\text{Li}_{\text{susp-diss}} = \delta^7\text{Li}_{\text{susp}} - \delta^7\text{Li}_{\text{diss}}$ ) across the Lena River watershed vary between -  
332 12.5 to -22.6 ‰. With the exception of the south-facing VMR sample with  $\Delta^7\text{Li}_{\text{susp-diss}} = -34.3\text{‰}$ , the  
333 narrow range of values do not allow for discrimination between the geographical regions. The  
334 magnitude of  $\Delta^7\text{Li}_{\text{susp-diss}}$  observed within the Lena River is comparable to values observed in rivers  
335 elsewhere ( $\Delta^7\text{Li}_{\text{susp-diss}} = -6$  to  $-36\text{‰}$ ; Huh et al., 2001; Kısakúrek et al., 2005; (Pogge von Strandmann  
336 et al., 2006; Pogge von Strandmann et al., 2010).

337

## 338 **5. Discussion**

339 The fractionation of Li isotopes is controlled by water-rock interactions during weathering  
340 processes, specifically the balance between release of Li during primary silicate rock dissolution,  
341 and the preferential incorporation or adsorption of  $^6\text{Li}$  during formation of secondary minerals  
342 (Pistiner and Henderson, 2003; Vigier et al., 2008; Wimpenny et al., 2010a). The variations in  $\delta^7\text{Li}_{\text{diss}}$

343 across the Lena River catchment reflect numerous complex processes occurring over the  
344 watershed. The lack of detailed observational data on the thermal regime for the individual  
345 catchment regions (e.g., active layer thaw depths, local microclimate, snow conditions, vegetation,  
346 soil properties, moisture content, lateral drainage, ground ice, etc.; Woo, 2012) complicates the  
347 interpretation of these isotopic variations to specific permafrost conditions. Here, we attempt to  
348 distinguish the dominant processes controlling Li isotope fractionation over such a large, complex,  
349 permafrost-dominated watershed.

350

### 351 **5.1 Sources of dissolved lithium**

352 Although carbonate weathering is the dominant contributor to total dissolved solids (TDS) in the  
353 Lena River catchment (Huh et al., 1998c; Huh et al., 1998b; Huh and Edmond, 1999), it contributes  
354 only a small fraction of the dissolved Li due to the low [Li] in carbonates. The possibility of inputs of  
355 Li from rainwater, ultimately derived from sea spray and so accompanied by other elements in the  
356 same proportions as in seawater, was investigated using the methods of Millot et al. (2010) and  
357 Dellinger et al. (2014) and a rainwater [Cl] after Gordeev et al. (1996). The range of measured Li/Cl  
358 ratios ( $1.6 \times 10^{-4}$  to  $7.9 \times 10^{-2}$ ) is much higher than the seawater ratio of  $5 \times 10^{-5}$ , and so a negligible  
359 (<5%) proportion of riverine Li originates from precipitation. Thus, the  $\delta^7\text{Li}$  data have not been  
360 corrected for these inputs, consistent with the approaches of other riverine studies (e.g. Millot et  
361 al., 2010; Bagard et al., 2015; Liu et al., 2015; Pogge von Strandmann et al., 2017).

362 Some of the rivers draining the CSP have elevated [Cl] and [SO<sub>4</sub><sup>-</sup>], which might be derived  
363 from weathering of evaporites that are abundant within the catchment region (Gordeev and  
364 Sidorov, 1993; Huh et al., 1998c; Yoon, 2010). However, as noted by Yoon (2010), this may also  
365 reflect a contribution from high [Cl] and [SO<sub>4</sub><sup>-</sup>] groundwaters. Using the same approach as Dellinger  
366 et al. (2014), and assuming evaporites have Li/Na =  $3 \times 10^{-5}$ , a low evaporite contribution has only  
367 been identified for a number of CSP (LR2013-50 (3%), LR2013-68 (8%), LR2013-79 (9%), LR2013-72  
368 (5%)); and Lena River main channel samples (LR2012-30, LR2012-32 and LR2013-48 (~5%); LR2012-  
369 31, LR2012-34 and LR2013-49 (~6%)). Overall therefore, the calculations show that dissolved Li is  
370 dominantly derived from the weathering of silicate material.

371

### 372 **5.2 Secondary mineralogical controls on Li isotope fractionation - Mineral saturation states**

373 The large range of Li isotope ratios observed in rivers has been proposed to reflect mineral-specific  
374 isotope fractionation factors controlled by the precipitation of (or interaction with) different

375 secondary mineral assemblages. This has been attributed to differences in bedrock lithology as well  
376 as weathering regime and hence weathering intensity, which control the water chemistry by  
377 removing major and trace elements from solution as the various secondary mineral phases  
378 precipitate (e.g., Millot et al., 2010; Wimpenny et al., 2010b; Pogge von Strandmann et al., 2006,  
379 2010).

380 In order to assess the likelihood and mineralogy of secondary mineral formation in the  
381 studied rivers, mineral saturation states were calculated with PHREEQC (Parkhurst and Appelo,  
382 1999), using the measured dissolved major cation and anion, Al and Fe concentrations, and *in-situ*  
383 pH, alkalinity and temperature data (after Hirst et al. 2017 and Sun et al. 2018).

384 The PHREEQC calculations indicate that in river samples from all of the geographical regions  
385 within the Lena River watershed, primary minerals such as quartz, olivine, pyroxene and feldspar  
386 are undersaturated and so are likely to be dissolving. In contrast, secondary minerals that are  
387 oversaturated ( $SI > 0$ ) in all rivers (and hence are likely to be precipitating) include amorphous and  
388 crystalline Fe oxyhydroxides (e.g., goethite, hematite, magnetite), Al oxides (e.g., gibbsite), Mn  
389 oxides (e.g., birnessite) and phyllosilicate minerals (e.g., K-mica, kaolinite, pyrophyllite). Smectite  
390 clay minerals (Ca- and Na-montmorillonite) and illite are only oversaturated within the Aldan and  
391 Lena Rivers (Supplementary Fig. 4). These waters were filtered using a 0.22  $\mu\text{m}$  cutoff, and so the  
392 oversaturation of amorphous Fe, Al and Mn oxides might reflect colloidal particles that have passed  
393 through the filter. These results are consistent with mineralogical assemblages determined by  
394 transmission electron microscopy (TEM) and synchrotron-based scanning transmission X-ray  
395 microscopy (STXM) identification of colloidal and suspended particulates for the same samples,  
396 which show abundant amorphous Fe(III) ferrihydrite on the sample filters (Hirst et al., 2017), and  
397 lesser crystalline goethite and hematite, along with clay minerals. There may also be secondary  
398 minerals, such as clays, that are inherited from weathering within the soil profile (Dellinger et al.,  
399 2014).

400 Links between Li isotope fractionation and specific secondary mineral saturation indices  
401 have been reported in basaltic terrains (Pogge von Strandmann et al., 2006, 2010), and in glacial  
402 rivers draining permafrost in west Greenland (Wimpenny et al., 2010b). In this study, however,  
403 there is no correlation between dissolved  $\delta^7\text{Li}$  and any PHREEQC calculated mineral saturation  
404 states (Supplementary Fig 3.). This is not unexpected for rivers draining large, multi-lithology  
405 catchments, where secondary mineralogy will also vary. Hence, whilst an abundance of amorphous  
406 and crystalline Fe oxides were observed in the secondary mineral phases on the filters for the

407 samples across the geographical regions throughout the Lena River watershed (Hirst et al., 2017),  
408 the presence of other secondary minerals (particularly clay minerals) are likely to have contributed  
409 to the  $\delta^7\text{Li}_{\text{susp}}$  due to the incorporation or sorption of  $^6\text{Li}$ .

410

### 411 **5.3 Topographical and catchment area controls on Li isotope fractionation**

412 Topography and relief can exert a strong influence on weathering. In regions unaffected by  
413 permafrost, topographically high regions are typically dominated by relatively high physical erosion  
414 with high denudation rates (often related to high uplift rates), and so high rates of exposure of fresh  
415 mineral surfaces and minimal water-rock interaction times (e.g., Montgomery and Brandon, 2002).  
416 This promotes the weathering of primary rock material and limits secondary mineral precipitation  
417 (low weathering intensity), and is expected to result in  $\delta^7\text{Li}$  compositions that approach those of  
418 the primary weathering rocks. In contrast, non-permafrost rivers in low-lying regions are expected  
419 to have higher  $\delta^7\text{Li}$  values, where greater water-rock interaction times promote the formation of  
420 secondary minerals and greater adsorption of Li, driving the riverine  $\delta^7\text{Li}$  towards higher values.  
421 This relationship has been suggested from a broad negative correlation between  $\delta^7\text{Li}$  and uplift rate  
422 in rivers from New Zealand (Pogge von Strandmann and Henderson, 2015) and in rivers draining  
423 higher elevations in the Ganges (Pogge von Strandmann et al., 2017) and the Amazon (Dellinger et  
424 al., 2015). This is also supported by generally low  $\delta^7\text{Li}$  observed in rivers in the High Himalayas (Huh  
425 et al., 1998a; Kısakúrek et al., 2005).

426 While uplift rates have not been directly quantified for the regions in this study, the mean  
427 gradient of the watershed can be used as a general measure of the overall relief. At low slope angles  
428 ( $<15^\circ$ ), a broad positive linear correlation has been shown between catchment slope angle and long-  
429 term erosion rate (Montgomery and Brandon, 2002). For catchments in the CSP, LAIRA and the VMR,  
430 the mean watershed gradient was calculated using a GIS-based approach as outlined in Kutscher et  
431 al. (2017), dividing the watershed length by its maximum elevation. While a meaningful watershed  
432 gradient cannot be estimated for the overall Lena, Aldan and Viliui River catchments, a watershed  
433 gradient has been estimated for the upper catchment regions draining in to the Viliui River (LR2013-  
434 62;  $0.96^\circ$ ) and Aldan River (LR2012-13;  $3.44^\circ$ ). Catchments of the low-lying CSP have catchment  
435 slope angles ranging from  $0.24$  to  $1.04^\circ$ . The LAIRA has catchment slope angles ranging from  $0.43$  to  
436  $1.65^\circ$ , and rivers draining the VMR range from  $0.94$  to  $6.34^\circ$ . Both [Li] and  $\delta^7\text{Li}_{\text{diss}}$  show little  
437 relationship with mean watershed gradient (Fig. 3). Despite the *ca.* five degree difference in slope  
438 angles between rivers draining the low-lying LAIRA and CSP, and the VMR, there is no clear

439 distinction between rivers draining the mountainous and the low-lying regions, with the entire  
440 range of [Li] and  $\delta^7\text{Li}_{\text{diss}}$  values spanning the full range of catchment slope angles. In fact, the highest  
441  $\delta^7\text{Li}_{\text{diss}}$  values observed in the Lena River watershed are from tributaries with the greatest slope  
442 angles draining the Verkhoyansk Mountain Ranges.

443 The lack of a trend between  $\delta^7\text{Li}$  and relief in the Lena River catchment may be due to  
444 cryogenic weathering processes prevalent in regions of continuous permafrost e.g., the continual  
445 supply of fresh primary minerals due to seasonal freeze/thaw cycles, frost shattering and salt  
446 weathering (Woo, 2012), none of which are directly related to relief (Goodfellow and  
447 Boelhouwers, 2013). Weathering rates can also be enhanced over predicted 'inorganic' weathering  
448 rates by organic acid weathering (Huh, 2003), and could also be a factor here.

449 The [Li] and  $\delta^7\text{Li}$  data are plotted against catchment area in Fig. 3. In general, discharge is  
450 expected to scale with increasing catchment area (Burgers et al., 2014). Whilst no trends can be  
451 seen between [Li] and catchment area (except in south-facing VMR rivers, as discussed below), a  
452 broad negative trend can be seen with Li isotope composition, with greater variability observed in  
453 smaller catchments, and isotopic compositions that approach the global mean value of  $\sim 23\text{‰}$  with  
454 larger catchment areas. This pattern likely reflects the dominance of local processes in smaller  
455 catchments, which are homogenised and integrated in rivers draining larger catchments.

456

#### 457 **5.4 Permafrost and climatic controls on Li isotope variations**

458 Since the Lena River watershed covers a vast area, the effects of climate on the distribution  
459 of Li isotopes can be considered. For this study, samples have been collected from a latitudinal and  
460 climate gradient from  $60^\circ$  to  $68^\circ$  N, corresponding to mean annual air temperatures (MAAT) of  $-6$   
461 to  $-15^\circ\text{C}$  (Gordeev and Sidorov, 1993). This corresponds to a range of maximum active layer  
462 temperatures, and so reaction rates for both dissolution and secondary mineral formation, as well  
463 as of depths and lengths of time of active layer thawing. To test the effects of temperature, and  
464 hence climate, [Li] and  $\delta^7\text{Li}_{\text{diss}}$  are shown plotted against latitude, used as a proxy for MAAT  
465 (Supplementary Fig. 5). The Lena River main channel  $\delta^7\text{Li}_{\text{diss}}$  values show a weak  $5\text{‰}$  increase from  
466 the upper to the lower reaches ( $R^2 = 0.47$ ) along the climate gradient. This progressive downstream  
467 increase in  $\delta^7\text{Li}_{\text{diss}}$  values observed in the Lena River main channel (Fig. 4a) is also observed in the  
468 Ganges (Bagard et al., 2015) and the Changjiang Rivers (Wang et al., 2015). After the confluence of  
469 the Viliui River, both Li concentrations and  $\delta^7\text{Li}_{\text{diss}}$  in the Lena River main channel increase (Fig. 4).  
470 This is unlikely to be simple mixing between the two rivers, because there are no trends between



471  $\delta^7\text{Li}_{\text{diss}}$  and  $1/[\text{Li}]$  (Fig. 2). Equally, anthropogenic influences from cities such as Yakutsk and Zhigansk  
472 do not appear to influence  $[\text{Li}]$  or  $\delta^7\text{Li}_{\text{diss}}$ . Thus, the evolution of the Lena River  $\delta^7\text{Li}_{\text{diss}}$  value likely  
473 reflects Li isotope fractionation due to precipitation or interaction with secondary minerals within  
474 the river, or local influences from groundwater or porewaters within permafrost soils.

475 Overall, there are also no clear trends in  $[\text{Li}]$  and  $\delta^7\text{Li}_{\text{diss}}$  values over a *ca.* nine degree latitude  
476 gradient, suggesting that variations in the MAAT, and thus climatic conditions, do not have a  
477 dominant influence on variations in  $\delta^7\text{Li}$  in the Lena River catchment. This is consistent with the  
478 results for rivers in Iceland (Pogge von Strandmann et al., 2010), rivers from different climatic zones  
479 of the Cascade Mountains (Colombia River Basalts; Liu et al., 2015) and the Mackenzie River basin  
480 (Millot et al., 2010). Interestingly, the greatest variation in both  $[\text{Li}]$  and  $\delta^7\text{Li}_{\text{diss}}$  are observed in the  
481 south-facing slopes draining the VMR. South-facing slopes in permafrost regions are typically  
482 characterised by increased summer insolation and higher daily temperatures which contribute to  
483 more rapid thawing of snow cover, warmer soils, greater active layer depth and hence greater  
484 infiltration of melt water (Woo, 2012; Hindshaw et al., 2018). Repeated freezing and thawing due  
485 to earlier snow melt can destabilise the soil cover, such that south-facing slopes are typically prone  
486 to greater hillslope instability (Vasiliev, 2009; Goodfellow and Boelhouwers, 2013). This may  
487 contribute towards local variations in water flow and hence different water-rock interaction times.  
488 The lower  $\delta^7\text{Li}_{\text{diss}}$  values observed in the VMR therefore likely reflect catchments dominated by  
489 lower intensity of weathering, enhanced dissolution of freshly exposed primary rock due to freeze-  
490 thaw processes and little fractionation of Li isotopes due to reduced secondary mineral  
491 precipitation or interaction with secondary minerals within the seasonally thawed active layer (i.e.,  
492 a weathering-limited regime). In contrast, the much higher  $\delta^7\text{Li}_{\text{diss}}$  values might reflect increased  
493 adsorption on secondary minerals, or dissolution/reprecipitation cycles due to repeated freeze-  
494 thaw cycles that promote greater water-rock interaction, significant secondary mineral formation  
495 and therefore greater Li isotope fractionation (i.e., high weathering intensity in a transport-limited  
496 regime). However, without detailed knowledge of the thermal regime in the individual catchments,  
497 it is difficult to speculate further on these processes. A detailed study of the cryogenic weathering  
498 processes occurring within a small, well-constrained river catchment draining continuous  
499 permafrost would shed some light on the relative importance of these contrasting processes.

500

501 **5.5 Modelled Rayleigh fractionation factors and water residence time - Li/Na**

502 Li and Na are both monovalent alkali metals that reside in primary silicate minerals, and are  
 503 readily mobilised into solution during weathering processes. During weathering, it is assumed that  
 504 Li and Na are released congruently, and the Li/Na ratio is progressively diminished by the  
 505 incremental removal of Li through interaction with secondary minerals that preferentially remove  
 506  ${}^6\text{Li}$ , either by adsorption onto the surface, by trapping within the interlayer (in the case of 2:1 clays),  
 507 or by incorporation into the mineral structure. This in turn increases  $\delta^7\text{Li}$  values and decreases Li/Na  
 508 values in waters. Values for  $\delta^7\text{Li}_{\text{diss}}$  are plotted against Li/Na ratios in Figure 5, where a broad  
 509 negative correlation between these two parameters is evident and similar to that observed in other  
 510 river systems (Millot et al., 2010; Bagard et al., 2015; Liu et al., 2015; Wang et al., 2015).

511 The relationship between Li removal into secondary minerals and associated Li isotope  
 512 fractionation was investigated using modelling approaches of other studies (Pogge von Strandmann  
 513 et al., 2010a; 2017; Bouchez et al., 2013; Dellinger et al., 2015; Bagard et al., 2015). One model  
 514 considers a water that initially has Li/Na and  $\delta^7\text{Li}$  values equal to those of weathering rocks, and  
 515 then is only progressively depleted by incremental loss of Li (while remaining well-mixed). In this  
 516 case, the value of  $\delta^7\text{Li}$  will increase as Li/Na decreases according to a Rayleigh distillation  
 517 relationship that is controlled by the fractionation factor ( $\alpha$ ) that reflects the preferential removal  
 518 of  ${}^6\text{Li}$ .

$$519 \quad \delta^7\text{Li}_{\text{diss}} = \delta^7\text{Li}_0 + 1000(\alpha-1)\ln(f_{\text{diss}}^{\text{Li}}) \quad (1)$$

520  
 521 where  $\delta^7\text{Li}_{\text{diss}}$  is the Li isotope composition of the dissolved phase and  $\delta^7\text{Li}_0$  is the value for Li  
 522 released into the water, equal to the mean  $\delta^7\text{Li}_{\text{rock}}$  of the weathered rocks. The term  $f_{\text{diss}}^{\text{Li}}$  is the  
 523 fraction of Li remaining in solution, calculated using the equation:

$$524 \quad f_{\text{diss}}^{\text{Li}} = \frac{\text{Li}/\text{Na}_{\text{diss}}}{\text{Li}/\text{Na}_0} \quad (2)$$

525  
 526 The fractionation lines represent the calculated compositions of waters subjected to different  
 527 degrees of Li removal from a single starting Li/Na and  $\delta^7\text{Li}$  composition. A starting isotopic  
 528 composition ( $\delta^7\text{Li}_0$ ) of 0‰ is used, which is a representative value for the average upper continental  
 529 crust. Changing  $\delta^7\text{Li}_0$  to values of -2 to +5‰ observed in riverine suspended sediments, shales and  
 530 upper continental crustal rocks and basalts will result in small shifts in the model curves (not  
 531 shown), although this will not substantially affect the range of fractionation factors needed to  
 532 explain the range of measured compositions. The bedrock Li/Na ratio (and hence the initial ratio of

533 Li/Na released into waters), is difficult to constrain for such a large, multi-lithological catchment  
534 and undoubtedly varies between sub-catchments and across the watershed. To account for a range  
535 of possible end-member values, a Li/Na<sub>0</sub> molar ratio of 0.03, equal to the highest dissolved value  
536 found in the Lena catchment area, and a value of 0.1, which is that of the upper continental crust  
537 (Taylor and McLennan, 1995) have been adopted in the model calculations. This range of initial  
538 Li/Na<sub>0</sub> are depicted by the grey box in Fig. 5.

539 The range of data within the Lena River catchment cannot be explained by a single isotopic  
540 fractionation factor. The majority of data fall within the curves for  $\alpha$  values ranging from  $\sim 0.997$  to  
541  $0.990$  ( $\Delta^7\text{Li} = -3\text{‰}$  and  $-10\text{‰}$ ). However, a number of outliers (particularly for rivers draining south-  
542 facing slopes within the VMR) fall outside these  $\alpha$  values, requiring a wider range of fractionation  
543 factors. The range of isotopic fractionation factors in Fig. 5 are consistent with experimentally  
544 determined values for various secondary minerals, including those predicted to be oversaturated  
545 within the Lena River (see section 5.2), with  $\alpha_{\text{vermiculite}} = 0.971$ ,  $\alpha_{\text{kaolinite}} = 0.979$ ,  $\alpha_{\text{gibbsite}} = 0.984-0.993$ ,  
546  $\alpha_{\text{ferrihydrite}} \approx 0.998$ , and  $\alpha_{\text{smectite}} = 0.984$  (Zhang et al. 1998; Pistiner and Henderson, 2003; Millot and  
547 Girard, 2007; Vigier et al. 2008; Wimpenny et al. 2015). The range of  $\alpha$  is also comparable to that  
548 those observed in other global rivers (e.g., Amazon (Dellinger et al., 2015); Ganges (Bagard et al.,  
549 2015; Pogge von Strandmann et al., 2017)). Overall, the range of fractionation factors required to  
550 explain the data reflects the complex behavior of Li in such a vast catchment. Variations are also  
551 expected from other processes, such as mixing between waters with different Li characteristics. In  
552 addition, variability may be caused by the uptake of Na into some secondary minerals (such as clays  
553 or zeolites), and/or desorption of Na from mineral surfaces in soils, thus decoupling Li/Na from  $\delta^7\text{Li}$ .  
554 It is not possible to distinguish whether these processes occur within the river, or is controlled by  
555 sub-surface residence time. It is likely that there are also other processes that have caused variations  
556 in Li/Na or  $\delta^7\text{Li}$  values, including mixing of porewaters within soils or groundwaters, as well as small  
557 scale variations in  $\delta^7\text{Li}$  and Li/Na values. Other interactions, including adsorption, precipitation in  
558 other phases, or interaction with organics, may also affect Li concentrations and possibly create  
559 further isotope fractionation.

560

## 561 **5.6 Comparison with global rivers**

562 Huh et al. (1998a) also measured dissolved  $\delta^7\text{Li}$  in the Lena River catchment, and several other  
563 Siberian rivers. They observed a wide range in  $\delta^7\text{Li}$  values ( $\sim 6$  to  $30\text{‰}$ ), similar to the values  
564 observed in this study. The dissolved  $\delta^7\text{Li}$  observed in the Lena River catchment (from this study

565 and Huh et al. 1998a) overlap with those of other polar, cold climate rivers that are underlain by  
566 continuous, discontinuous, sporadic or isolated permafrost (e.g., the Mackenzie River basin (~9 to  
567 29‰; Millot et al., 2010), Spitzbergen (~8 to 14‰; Hindshaw et al., 2018) and Antarctic rivers (~12  
568 to 23‰; Witherow et al., 2010)). They also overlap with values from glaciated and non-glaciated  
569 rivers in west Greenland that are underlain by permafrost (~14 to 36‰; Wimpenny et al., 2010b),  
570 and those of rivers in Iceland that are unaffected by permafrost (~10 to 44‰; Pogge von  
571 Strandmann et al., 2006; Vigier et al., 2009).

572 Interestingly, the overall range in  $\delta^7\text{Li}$  and Li/Na values in these cold climate, polar regions  
573 (including regions impacted by permafrost and glacial weathering processes) are similar to those  
574 found in temperate and tropical rivers (Fig. 6). It has been proposed that weathering rates are  
575 strongly controlled by temperature and hence climate (precipitation and runoff) (e.g. West et al.,  
576 2005; Gislason et al., 2009). Warmer, wetter watersheds are expected to have greater chemical  
577 weathering rates than watersheds in high latitude permafrost-dominated regions, where the cold  
578 climate and restricted water-rock and water-soil interactions are predicted to reduce the extent of  
579 chemical weathering (Huh and Edmond, 1999). Whilst Li isotopes cannot constrain the rates of  
580 silicate weathering (for a discussion, see Pogge von Strandmann et al., 2017), the magnitude of Li  
581 isotope fractionation, and hence intensity of weathering (i.e., the rate of secondary mineral  
582 formation relative to the rate of primary mineral dissolution) observed in such cold climate, polar  
583 regions is partly due to the increased supply of Li from primary minerals due to enhanced physical  
584 erosion facilitating greater chemical weathering. The unique role of cryogenic weathering  
585 processes such as repeat freeze-thaw cycles, frost shattering and salt weathering continually  
586 expose fresh primary minerals and prevents the accumulation of weathered products and  
587 development of thick soil profiles. The high degree of physical erosion, together with enhanced  
588 chemical weathering by the presence of organic acids is sufficient to overcome the temperature  
589 inhibition on the mineral reaction kinetics (Huh et al., 1998b,c; Huh and Edmond, 1999; Woo, 2012).

590 Global rivers are further compared in Figure 7, which shows the frequency of dissolved Li  
591 isotope data for some of the large global rivers and rivers draining basaltic terrains. Typically, the  
592 Ganges, Lena and basalts all have similar frequency peaks, clustering around the global riverine  
593 mean of ~23‰ (Huh et al., 1998a). Rivers draining the high Himalayas have a slightly lower average  
594 value (~14 to 16‰), consistent with greater exposure rates of fresh rock driving the Li isotopic  
595 compositions towards crustal rock values. Interestingly, the Amazon and Mackenzie Rivers have the  
596 lightest mean values of these large datasets, of ~16‰. Hence, the mean values of these different

597 catchments are quite similar relative to the overall variability in  $\delta^7\text{Li}$  observed in rivers. This, in  
598 combination with the trends with Li/Na, further supports the conclusion that climatic controls (e.g.,  
599 temperature and runoff) are weak secondary controls on Li isotopes and hence silicate weathering  
600 processes of primary rock dissolution relative to secondary mineral formation. The data therefore  
601 suggest that similar processes control global Li geochemistry in rivers from cold, temperate and  
602 tropical regions.

603 This has implications for the use of  $\delta^7\text{Li}$  as a palaeo-weathering tracer, because it implies  
604 that the global riverine mean of 23‰ is not the result of mixing Li with a wide range of  $\delta^7\text{Li}$  values  
605 in different rivers (as it is, for example, for  $^{87}\text{Sr}/^{86}\text{Sr}$ ; Palmer and Edmond, 1989), but rather that  
606 many major rivers share a value of  $\sim 23\text{‰}$ , irrespective of climate and weathering regime. This  
607 therefore suggests that in order to explain the  $\delta^7\text{Li}_{\text{seawater}} \sim 9\text{‰}$  increase observed during the early  
608 Cenozoic (Hathorne and James, 2006; Misra and Froelich, 2012), the global weathering conditions  
609 would have to have significantly changed from low weathering intensity conditions imparting low  
610 riverine  $\delta^7\text{Li}_{\text{diss}}$  input to the oceans, to the present day weathering conditions imparting a mean  
611 riverine  $\delta^7\text{Li}_{\text{diss}}$  of 23‰. Hence, if the global riverine  $\delta^7\text{Li}$  is not principally controlled by climate, this  
612 may suggest that the Cenozoic Li curve may be more significantly controlled by changing riverine  
613 fluxes, rather than isotope ratios, possibly coupled with changes associated with the removal of Li  
614 from the oceans (Li and West, 2014; Coogan et al., 2017).

615

## 616 **6. Conclusions**

617 In this study, we report Li data for over 70 river waters and 11 suspended sediments from the Lena  
618 River Basin, a large, complex, multi-lithological catchment underlain by continuous permafrost  
619 discharging into the Arctic Ocean. A fractionation factor ( $\alpha$ ) during weathering of between  $\sim 0.997$   
620 and 0.990 can explain the data for the Lena River, comparable to previously published experimental  
621 and field based values from highly disparate climates and weathering regimes. Contrary to reports  
622 from other studies from rivers in non-permafrost terrains, there are no systematic trends observed  
623 between riverine  $\delta^7\text{Li}_{\text{diss}}$  and watershed mean slope angle (a proxy for erosion rate), and so between  
624 values for rivers draining the Verkhyansk Mountain Range (VMR) when compared to those for low-  
625 lying rivers of the Central Siberian Plateau. South-facing catchments from the VMR do exhibit more  
626  $\delta^7\text{Li}$  variation than other areas, likely due to the higher insolation affecting the size of the active  
627 layer. Overall, cryogenic weathering processes found in permafrost-dominated regions seasonally  
628 likely provide a fresh supply of unweathered primary silicate rock material (due to freeze-thaw

629 processes), which would lower dissolved  $\delta^7\text{Li}$ . Combined with organic acids that enhance chemical  
630 weathering (despite low temperatures hindering weathering rates) and promote secondary  
631 mineral formation. Together, these weathering features prevalent within regions of continuous  
632 permafrost may obscure any topographical controls on Li isotope fractionation observed in rivers  
633 draining non-permafrost.

634 At the basin scale, the Lena River has a remarkably similar range in  $\delta^7\text{Li}$  values to global rivers  
635 from contrasting climate and weathering regimes from polar, temperate and tropical regions.  
636 Overall, temperature, the presence of permafrost, and indeed climate are weak controls on riverine  
637 Li isotope compositions, and similar processes (that is, the balance between primary silicate mineral  
638 dissolution and the preferential incorporation or adsorption of  $^6\text{Li}$  during formation of secondary  
639 minerals) that operate in different climates control global riverine Li geochemistry. This suggests  
640 that climate changes likely will little affect the isotope composition of Li delivered to the ocean, and  
641 changing riverine flux must be considered when using sedimentary records of Li isotopes to  
642 understand changes in past weathering regimes (e.g. Pogge von Strandmann et al., 2017b).

643

#### 644 **Acknowledgements**

645 This project was funded by the Swedish Research Council (VR 621-2010-3917), the Swedish Polar  
646 Research Secretariat (SIMO 2011-165 and 2012-213) and MetTrans, an EU FP7 Marie Curie Initial  
647 Training Network grant. We would like to thank Phil Holdship for his assistance with trace element  
648 analysis, Yu-Te (Alan) Hsieh for help with the MC-ICP-MS and Jon Wade for assistance with data  
649 presentation. We also thank Fang-Zhen Teng (*associate editor*), Josh Wimpenny, and two  
650 anonymous reviewers for constructive comments on an earlier version of the manuscript. PPvS and  
651 MJM are supported by ERC Consolidator grant 682760 - CONTROLPASTCO2.

652

#### 653 **References**

654

- 655 Bagard M.-L., West A. J., Newman K. and Basu A. R. (2015) Lithium isotope fractionation in the  
656 Ganges–Brahmaputra floodplain and implications for groundwater impact on seawater  
657 isotopic composition. *Earth Planet. Sci. Lett.* **432**, 404–414.
- 658 Berner R. A., Lasaga A. C. and Garrels R. M. (1983) The carbonate-silicate geochemical cycle and its  
659 effect on atmospheric carbon dioxide over the past 100 million years. *Am. J. Sci.* **283**, 641–  
660 683.
- 661 Bouchez J., von Blanckenburg F. and Schuessler J. A. (2013) Modeling novel stable isotope ratios in  
662 the weathering zone. *Am. J. Sci.* **313**, 267–308.

- 663 Bouchez J., Gaillardet J., France-Lanord C., Maurice L. and Dutra-Maia P. (2011) Grain size control  
664 of river suspended sediment geochemistry: Clues from Amazon River depth profiles.  
665 *Geochemistry, Geophys. Geosystems* **12**.
- 666 Burgers H. E. (Robin), Schipper A. M. and Jan Hendriks A. (2014) Size relationships of water  
667 discharge in rivers: scaling of discharge with catchment area, main-stem length and  
668 precipitation. *Hydrol. Process.* **28**, 5769–5775.
- 669 Chan L. H., Edmond J. M., Thompson G. and Gillis K. (1992) Lithium isotopic composition of  
670 submarine basalts: implications for the lithium cycle in the oceans. *Earth Planet. Sci. Lett.* **108**,  
671 151–160.
- 672 Chevychelov A. P. and Bosikov N. P. (2010) Natural Conditions BT - The Far North: Plant  
673 Biodiversity and Ecology of Yakutia. In (eds. E. I. Troeva, A. P. Isaev, M. M. Cherosov, and N. S.  
674 Karpov). Springer Netherlands, Dordrecht. pp. 1–23.
- 675 Coogan L. A., Gillis K. M., Pope M. and Spence J. (2017) The role of low-temperature (off-axis)  
676 alteration of the oceanic crust in the global Li-cycle: Insights from the Troodos ophiolite.  
677 *Geochim. Cosmochim. Acta* **203**, 201–215.
- 678 Dellinger M., Bouchez J., Gaillardet J., Faure L. and Moureau J. (2017) Tracing weathering regimes  
679 using the lithium isotope composition of detrital sediments. *Geol.* **45**, 411–414.
- 680 Dellinger M., Gaillardet J., Bouchez J., Calmels D., Galy V., Hilton R. G., Louvat P. and France-Lanord  
681 C. (2014) Lithium isotopes in large rivers reveal the cannibalistic nature of modern  
682 continental weathering and erosion. *Earth Planet. Sci. Lett.* **401**, 359–372.
- 683 Dellinger M., Gaillardet J., Bouchez J., Calmels D., Louvat P., Dosseto A., Gorge C., Alanoca L. and  
684 Maurice L. (2015) Riverine Li isotope fractionation in the Amazon River basin controlled by  
685 the weathering regimes. *Geochim. Cosmochim. Acta* **164**, 71–93.
- 686 Eiriksdottir E. S., Gislason S. R. and Oelkers E. H. (2013) Does temperature or runoff control the  
687 feedback between chemical denudation and climate? Insights from NE Iceland. *Geochim.*  
688 *Cosmochim. Acta* **107**, 65–81.
- 689 Elliott T., Thomas A., Jeffcoate A. and Niu Y. (2006) Lithium isotope evidence for subduction-  
690 enriched mantle in the source of mid-ocean-ridge basalts. *Nature* **443**, 565–568.
- 691 Fedorov A. N., Ivanova R. N., Park H., Hiyama T. and Iijima Y. (2014) Recent air temperature  
692 changes in the permafrost landscapes of northeastern Eurasia. *Polar Sci.* **8**, 114–128.
- 693 Flesch G. D., Anderson A. R. and Svec H. J. (1973) A secondary isotopic standard for  $6\text{Li}/7\text{Li}$   
694 determinations. *Int. J. Mass Spectrom. Ion Phys.* **12**, 265–272.
- 695 Frey K. E. and McClelland J. W. (2009) Impacts of permafrost degradation on arctic river  
696 biogeochemistry. *Hydrol. Process.* **23**, 169–182.
- 697 Frings P. J., Clymans W., Fontorbe G., Gray W., Chakrapani G. J., Conley D. J. and De La Rocha C.  
698 (2015) Silicate weathering in the Ganges alluvial plain. *Earth Planet. Sci. Lett.* **427**, 136–148.
- 699 Frings P. J., Clymans W., Fontorbe G., Rocha C. L. D. La and Conley D. J. (2016) The continental Si  
700 cycle and its impact on the ocean Si isotope budget. *Chem. Geol.* **425**, 12–36.
- 701 Georg R. B., Reynolds B. C., West A. J., Burton K. W. and Halliday A. N. (2007) Silicon isotope  
702 variations accompanying basalt weathering in Iceland. *Earth Planet. Sci. Lett.* **261**, 476–490.
- 703 Georg R. B., West A. J., Basu A. R. and Halliday A. N. (2009) Silicon fluxes and isotope composition  
704 of direct groundwater discharge into the Bay of Bengal and the effect on the global ocean  
705 silicon isotope budget. *Earth Planet. Sci. Lett.* **283**, 67–74.
- 706 Gislason S. R., Arnorsson S. and Armannsson H. (1996) Chemical weathering of basalt in Southwest  
707 Iceland; effects of runoff, age of rocks and vegetative/glacial cover. *Am. J. Sci.* **296**, 837–907.
- 708 Goodfellow B. W. and Boelhouwers J. (2013) 7.31 Hillslope Processes in Cold Environments: An  
709 Illustration of High-Latitude Mountain and Hillslope Processes and Forms. In *Treatise on*

710 *Geomorphology* (ed. J. F. Shroder). Academic Press, San Diego. pp. 320–336.

711 Gordeev V. V, Martin J. M., Sidorov I. S. and Sidorova M. V (1996) A reassessment of the Eurasian  
712 river input of water, sediment, major elements, and nutrients to the Arctic Ocean. *Am. J. Sci.*  
713 **296**, 664–691.

714 Gordeev V. V and Sidorov I. S. (1993) Concentrations of major elements and their outflow into the  
715 Laptev Sea by the Lena River. *Mar. Chem.* **43**, 33–45.

716 Hathorne E. C. and James R. H. (2006) Temporal record of lithium in seawater: A tracer for silicate  
717 weathering? *Earth Planet. Sci. Lett.* **246**, 393–406.

718 Henchiri S., Gaillardet J., Dellinger M., Bouchez J. and Spencer R. G. M. (2016) Temporal variations  
719 of riverine dissolved lithium isotopic signatures unveil contrasting weathering regimes in low-  
720 relief Central Africa. *Geophys. Res. Lett.* **43**.

721 Hilley G. E., Chamberlain C. P., Moon S., Porder S. and Willett S. D. (2010) Competition between  
722 erosion and reaction kinetics in controlling silicate-weathering rates., *Earth Planet. Sci. Lett.*  
723 **293**, 191–199.

724 Hirst C., Andersson P. S., Shaw S., Burke I. T., Kutscher L., Murphy M. J., Maximov T., Pokrovsky O.  
725 S., Mörth C.-M. and Porcelli D. (2017) Characterisation of Fe-bearing particles and colloids in  
726 the Lena River basin, NE Russia. *Geochim. Cosmochim. Acta* **213**, 553–573.

727 Holmes R. M., McClelland J. W., Tank S. E., Spencer R. G. M. and Shiklomanov A. I. (2018) Arctic  
728 Great Rivers Observatory. Water Quality Dataset Version 20180321. Available at:  
729 <https://www.arcticgreatrivers.org/data>.

730 Huh Y. (2003) Chemical weathering and climate --- a global experiment: A review. *Geosci. J.* **7**,  
731 277–288.

732 Huh Y., Chan L.-H. and Edmond J. M. (2001) Lithium isotopes as a probe of weathering processes:  
733 Orinoco River. *Earth Planet. Sci. Lett.* **194**, 189–199.

734 Huh Y., Chan L.-H., Zhang L. and Edmond J. M. (1998a) Lithium and its isotopes in major world  
735 rivers: implications for weathering and the oceanic budget. *Geochim. Cosmochim. Acta* **62**,  
736 2039–2051.

737 Huh Y. and Edmond J. M. (1999) The fluvial geochemistry of the rivers of Eastern Siberia: III.  
738 Tributaries of the Lena and Anabar draining the basement terrain of the Siberian Craton and  
739 the Trans-Baikal Highlands. *Geochim. Cosmochim. Acta* **63**, 967–987.

740 Huh Y., Panteleyev G., Babich D., Zaitsev A. and Edmond J. M. (1998b) The fluvial geochemistry of  
741 the rivers of Eastern Siberia: II. Tributaries of the Lena, Omoloy, Yana, Indigirka, Kolyma, and  
742 Anadyr draining the collisional/accretionary zone of the Verkhoyansk and Cherskiy ranges.  
743 *Geochim. Cosmochim. Acta* **62**, 2053–2075.

744 Huh Y., Tsoi M.-Y., Zaitsev A. and Edmond J. M. (1998c) The fluvial geochemistry of the rivers of  
745 Eastern Siberia: I. tributaries of the Lena River draining the sedimentary platform of the  
746 Siberian Craton. *Geochim. Cosmochim. Acta* **62**, 1657–1676.

747 Kısakürek B., James R. H. and Harris N. B. W. (2005) Li and  $\delta^7\text{Li}$  in Himalayan rivers: Proxies for  
748 silicate weathering? *Earth Planet. Sci. Lett.* **237**, 387–401.

749 Kutscher L., Mörth C.-M., Porcelli D., Hirst C., Maximov T. C., Petrov R. E. and Andersson P. S.  
750 (2017) Spatial variation in concentration and sources of organic carbon in the Lena River,  
751 Siberia. *J. Geophys. Res. Biogeosciences* **122**, 1999–2016.

752 Lemarchand E., Schott J. and Gaillardet J. (2007) How surface complexes impact boron isotope  
753 fractionation: Evidence from Fe and Mn oxides sorption experiments. *Earth Planet. Sci. Lett.*  
754 **260**, 277–296.

755 Li G. and West A. J. (2014) Evolution of Cenozoic seawater lithium isotopes: Coupling of global  
756 denudation regime and shifting seawater sinks. *Earth Planet. Sci. Lett.* **401**, 284–293.



- 757 Available at: <http://www.sciencedirect.com/science/article/pii/S0012821X14003884>.
- 758 Liu C.-Q., Zhao Z.-Q., Wang Q. and Gao B. (2011) Isotope compositions of dissolved lithium in the  
759 rivers Jinshajiang, Lancangjiang, and Nujiang: Implications for weathering in Qinghai-Tibet  
760 Plateau. *Appl. Geochemistry* **26**, S357–S359.
- 761 Liu X.-M., Wanner C., Rudnick R. L. and McDonough W. F. (2015) Processes controlling  $\delta^7\text{Li}$  in  
762 rivers illuminated by study of streams and groundwaters draining basalts. *Earth Planet. Sci.*  
763 *Lett.* **409**, 212–224.
- 764 Manaka T., Araoka D., Yoshimura T., Hossain H. M. Z., Nishio Y., Suzuki A. and Kawahata H. (2017)  
765 Downstream and seasonal changes of lithium isotope ratios in the Ganges-Brahmaputra river  
766 system. *Geochemistry, Geophys. Geosystems* **18**, 3003–3015.
- 767 Millot R., Gaillardet J. érôme, Dupré B. and Allègre C. J. (2003) Northern latitude chemical  
768 weathering rates: clues from the Mackenzie River Basin, Canada. *Geochim. Cosmochim. Acta*  
769 **67**, 1305–1329.
- 770 Millot R. and Girard J. P. (2007) Lithium Isotope Fractionation during adsorption onto mineral  
771 surfaces. In *Clays in natural & engineered barriers for radioactive waste confinement. 3rd*  
772 *International meeting* Lille, France.
- 773 Millot R., Vigier N. and Gaillardet J. (2010) Behaviour of lithium and its isotopes during weathering  
774 in the Mackenzie Basin, Canada. *Geochim. Cosmochim. Acta* **74**, 3897–3912.
- 775 Misra S. and Froelich P. N. (2012) Lithium Isotope History of Cenozoic Seawater: Changes in Silicate  
776 Weathering and Reverse Weathering. *Science (80-. )*. **335**, 818–823.
- 777 Montgomery D. R. and Brandon M. T. (2002) Topographic controls on erosion rates in tectonically  
778 active mountain ranges. *Earth Planet. Sci. Lett.* **201**, 481–489.
- 779 Nezat C. A., Lyons W. B. and Welch K. A. (2001) Chemical weathering in streams of a polar desert  
780 (Taylor Valley, Antarctica). *Geol. Soc. Am. Bull.* **113**, 1401–1408.
- 781 Opfergelt S., Burton K. W., Pogge von Strandmann P. A. E., Gislason S. R. and Halliday A. N. (2013)  
782 Riverine silicon isotope variations in glaciated basaltic terrains: Implications for the Si delivery  
783 to the ocean over glacial–interglacial intervals. *Earth Planet. Sci. Lett.* **369–370**, 211–219.
- 784 Palmer M. R. and Edmond J. M. (1989) The strontium isotope budget of the modern ocean. *Earth*  
785 *Planet. Sci. Lett.* **92**, 11–26.
- 786 Parkhurst D. L. and Appelo C. A. J. (1999) *User's guide to PHREEQC (Version 2): a computer*  
787 *program for speciation, batch-reaction, one-dimensional transport, and inverse geochemical*  
788 *calculations.*,
- 789 Pistiner J. S. and Henderson G. M. (2003) Lithium-isotope fractionation during continental  
790 weathering processes. *Earth Planet. Sci. Lett.* **214**, 327–339.
- 791 Pogge von Strandmann P. A. E., Burton K. W., James R. H., van Calsteren P. and Gislason, S. R.  
792 (2010a) Assessing the role of climate on uranium and lithium isotope behaviour in rivers  
793 draining a basaltic terrain. *Chem. Geol.* **270**, 227–239.
- 794 Pogge von Strandmann P. A. E., Burton K. W., James R. H., van Calsteren P., Gíslason S. R. and  
795 Mokadem F. (2006) Riverine behaviour of uranium and lithium isotopes in an actively  
796 glaciated basaltic terrain. *Earth Planet. Sci. Lett.* **251**, 134–147.
- 797 Pogge von Strandmann P. A. E., Burton K. W., Opfergelt S., Eiríksdóttir E. S., Murphy M. J.,  
798 Einarsson A. and Gislason S. R. (2016) The effect of hydrothermal spring weathering  
799 processes and primary productivity on lithium isotopes: Lake Myvatn, Iceland. *Chem. Geol.*
- 800 Pogge von Strandmann P. A. E., Elliott T., Marschall H. R., Coath C., Lai Y.-J., Jeffcoate A. B. and  
801 Ionov D. A. (2011) Variations of Li and Mg isotope ratios in bulk chondrites and mantle  
802 xenoliths. *Geochim. Cosmochim. Acta* **75**, 5247–5268.
- 803 Pogge von Strandmann P. A. E., Frings P. J. and Murphy M. J. (2017) Lithium isotope behaviour

804 during weathering in the Ganges Alluvial Plain. *Geochim. Cosmochim. Acta* **198**, 17–31.

805 Pogge von Strandmann P. A. E. and Henderson G. M. (2015) The Li isotope response to mountain  
806 uplift. *Geology* **43**, 67–70.

807 Pogge von Strandmann P. A. E., James R. H., van Calsteren P. and Gislason S. R. (2010b) Assessing  
808 the role of climate on uranium and lithium isotope behaviour in rivers draining a basaltic  
809 terrain. *Chem. Geol.* **270**, 227–239.

810 Pogge von Strandmann P. A. E., Jenkyns H. C. and Woodfine R. G. (2013) Lithium isotope evidence  
811 for enhanced weathering during Oceanic Anoxic Event 2. *Nat. Geosci* **6**, 668–672.

812 Pokrovsky O. S., Schott J., Kudryavtzev D. I. and Dupré B. (2005) Basalt weathering in Central  
813 Siberia under permafrost conditions. *Geochim. Cosmochim. Acta* **69**, 5659–5680.

814 Raymo M. E. and Ruddiman W. F. (1992) Tectonic forcing of late Cenozoic climate. *Nature* **359**,  
815 117–122.

816 Raymo M. E., Ruddiman W. F. and Froelich P. N. (1988) Influence of late Cenozoic mountain  
817 building on ocean geochemical cycles. *Geol.* **16**, 649–653.

818 Sauzéat L., Rudnick R. L., Chauvel C., Garçon M. and Tang M. (2015) New perspectives on the Li  
819 isotopic composition of the upper continental crust and its weathering signature. *Earth  
820 Planet. Sci. Lett.* **428**, 181–192.

821 Stallard R. F. and Edmond J. M. (1983) Geochemistry of the Amazon: 2. The influence of geology  
822 and weathering environment on the dissolved load. *J. Geophys. Res. Ocean.* **88**, 9671–9688.

823 Stefánsson A., Gíslason S. R. and Arnórsson S. (2001) Dissolution of primary minerals in natural  
824 waters: II. Mineral saturation state. *Chem. Geol.* **172**, 251–276.

825 Sun X., Mörth C.-M., Porcelli D., Kutscher L., Hirst C., Murphy M. J., Maximov T., Petrov R. E.,  
826 Humborg C., Schmitt M. and Andersson P. S. Stable Silicon Isotopic Compositions of the Lena  
827 River and its Tributaries: Implications for Silicon Delivery to the Arctic Ocean. *Geochim.  
828 Cosmochim. Acta*.

829 Taylor S. R. and McLennan S. M. (1995) The geochemical evolution of the continental crust. *Rev.  
830 Geophys.* **33**, 241–265.

831 Teng F.-Z., McDonough W. F., Rudnick R. L., Dalpé C., Tomascak P. B., Chappell B. W. and Gao S.  
832 (2004) Lithium isotopic composition and concentration of the upper continental crust.  
833 *Geochim. Cosmochim. Acta* **68**, 4167–4178.

834 Tomascak P. B., Langmuir C. H., le Roux P. J. and Shirey S. B. (2008) Lithium isotopes in global mid-  
835 ocean ridge basalts. *Geochim. Cosmochim. Acta* **72**, 1626–1637.

836 Vasiliev I. S. (2009) Mountain permafrost landscapes of Yakutia. *Geogr. Nat. Resour.* **30**, 92–95.

837 Viers, J., Prokushkin, A.S., Pokrovsky, O.S., Auda, Y., Kirilyanov, A.D., Beaulieu, E., Zouiten, C., Oliva,  
838 P., Dupré, B., (2012) Seasonal and spatial variability of elemental concentrations in boreal  
839 forest larch foliage of Central Siberia on continuous permafrost. *Biogeochemistry* **xx(xx)**, pp-  
840 pp.

841 Vigier N., Decarreau A., Millot R., Carignan J., Petit S. and France-Lanord C. (2008) Quantifying Li  
842 isotope fractionation during smectite formation and implications for the Li cycle. *Geochim.  
843 Cosmochim. Acta* **72**, 780–792.

844 Vigier N., Gislason S. R., Burton K. W., Millot R. and Mokadem F. (2009) The relationship between  
845 riverine lithium isotope composition and silicate weathering rates in Iceland. *Earth Planet. Sci.  
846 Lett.* **287**, 434–441.

847 Vigier N. and Goddérís Y. (2015) A new approach for modeling Cenozoic oceanic lithium isotope  
848 paleo-variations: the key role of climate. *Clim. Past* **11**, 635–645.

849 Walker J. C. G., Hays P. B. and Kasting J. F. (1981) A negative feedback mechanism for the long-  
850 term stabilization of Earth's surface temperature. *J. Geophys. Res.* **86**, 9776.

851 Wang Q.-L., Chetelat B., Zhao Z.-Q., Ding H., Li S.-L., Wang B.-L., Li J. and Liu X.-L. (2015) Behavior  
852 of lithium isotopes in the Changjiang River system: Sources effects and response to  
853 weathering and erosion. *Geochim. Cosmochim. Acta* **151**, 117–132.

854 West A. J., Galy A. and Bickle M. (2005) Tectonic and climatic controls on silicate weathering. *Earth*  
855 *Planet. Sci. Lett.* **235**, 211–228.

856 Weynell M., Wiechert U. and Schuessler J. A. (2017) Lithium isotopes and implications on chemical  
857 weathering in the catchment of Lake Donggi Cona, northeastern Tibetan Plateau. *Geochim.*  
858 *Cosmochim. Acta* **213**, 155–177.

859 Wimpenny J., Colla C. A., Yu P., Yin Q. Z., Rustad J. R. and Casey W. H. (2015) Lithium isotope  
860 fractionation during uptake by gibbsite. *Geochim. Cosmochim. Acta* **168**.

861 Wimpenny J., Gisalason S.R., James R.H., Gannoun A., Pogge von Strandmann P.A.E., Burton K.W.  
862 (2010a) The behaviour of Li and Mg isotopes during primary phase dissolution and sec-  
863 ondary mineral formation in basalt. *Geochim. Cosmochim. Acta* **74**, 5259–5279.

864 Wimpenny J., James R. H., Burton K. W., Gannoun A., Mokadem F. and Gíslason S. R. (2010b)  
865 Glacial effects on weathering processes: New insights from the elemental and lithium isotopic  
866 composition of West Greenland rivers. *Earth Planet. Sci. Lett.* **290**, 427–437.

867 Witherow R. A., Lyons W. B. and Henderson G. M. (2010) Lithium isotopic composition of the  
868 McMurdo Dry Valleys aquatic systems. *Chem. Geol.* **275**, 139–147.

869 Woo, M. K. (2012). Permafrost hydrology. Springer Science & Business Media.

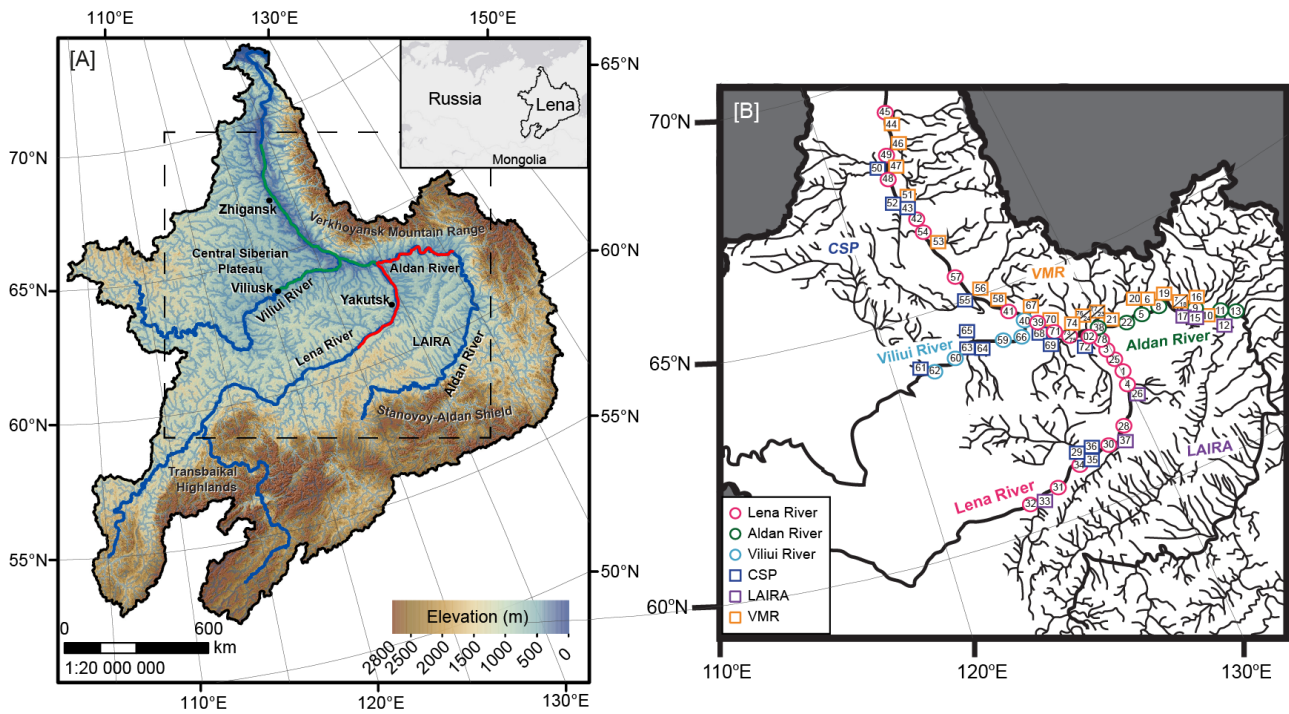
870 Yang, D., Kane, D., Hinzman, L., Zhang, X., Zhang, T. & Ye, H. 2002. Siberian Lena river hydrologic  
871 regime and recent change. *J. Geophys. Res.* **107**(D23): 4694.

872 Ye B., Yang D. and Kane D. L. (2003) Changes in Lena River streamflow hydrology: Human impacts  
873 versus natural variations. *Water Resour. Res.* **39**.

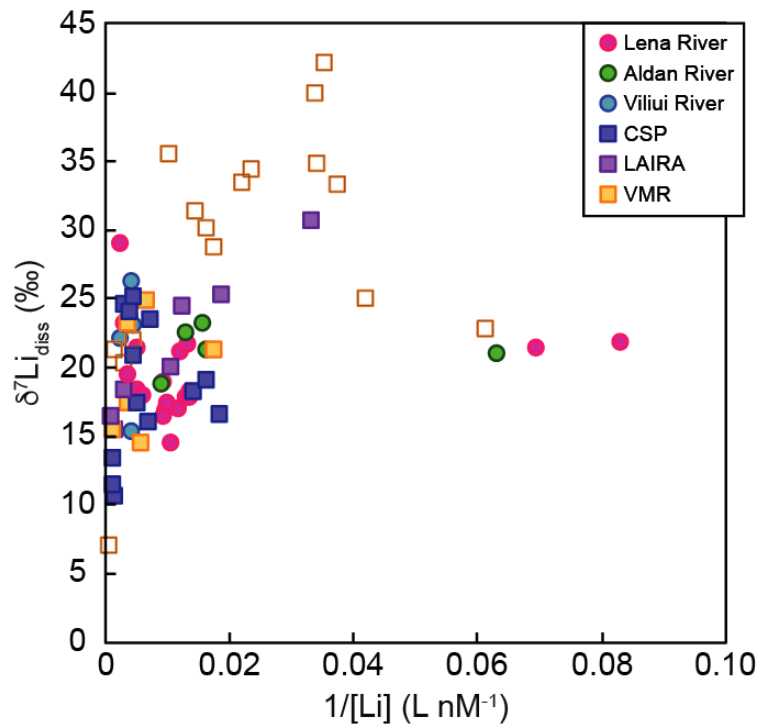
874 Yoon J. (2010) Lithium as a Silicate Weathering Proxy: Problems and Perspectives. *Aquat.*  
875 *Geochemistry* **16**, 189–206.

876 Zhang L., Chan L.-H. and Gieskes J. M. (1998) Lithium isotope geochemistry of pore waters from  
877 ocean drilling program Sites 918 and 919, Irminger Basin. *Geochim. Cosmochim. Acta* **62**,  
878 2437–2450.

879  
880



884 Figure 1: Map showing the Lena River catchment and its sub-catchment regions with the July 2012  
 885 sampling route shown in red and June 2013 in green in panel A. In panel B, sampling locations are  
 886 shown, with those within the Lena River main channel or the Viliui and Aldan Rivers, which are major  
 887 tributaries, denoted by circles. Smaller tributaries of the Central Siberian Plateau (CSP), Lena-  
 888 Amginsky inter-river area (LAIRA) and Verkhoyansk Mountain Range (VMR) are denoted by squares  
 889 (maps modified after Hirst et al. 2017). The same symbols and colour scheme are used in subsequent  
 890 figures.

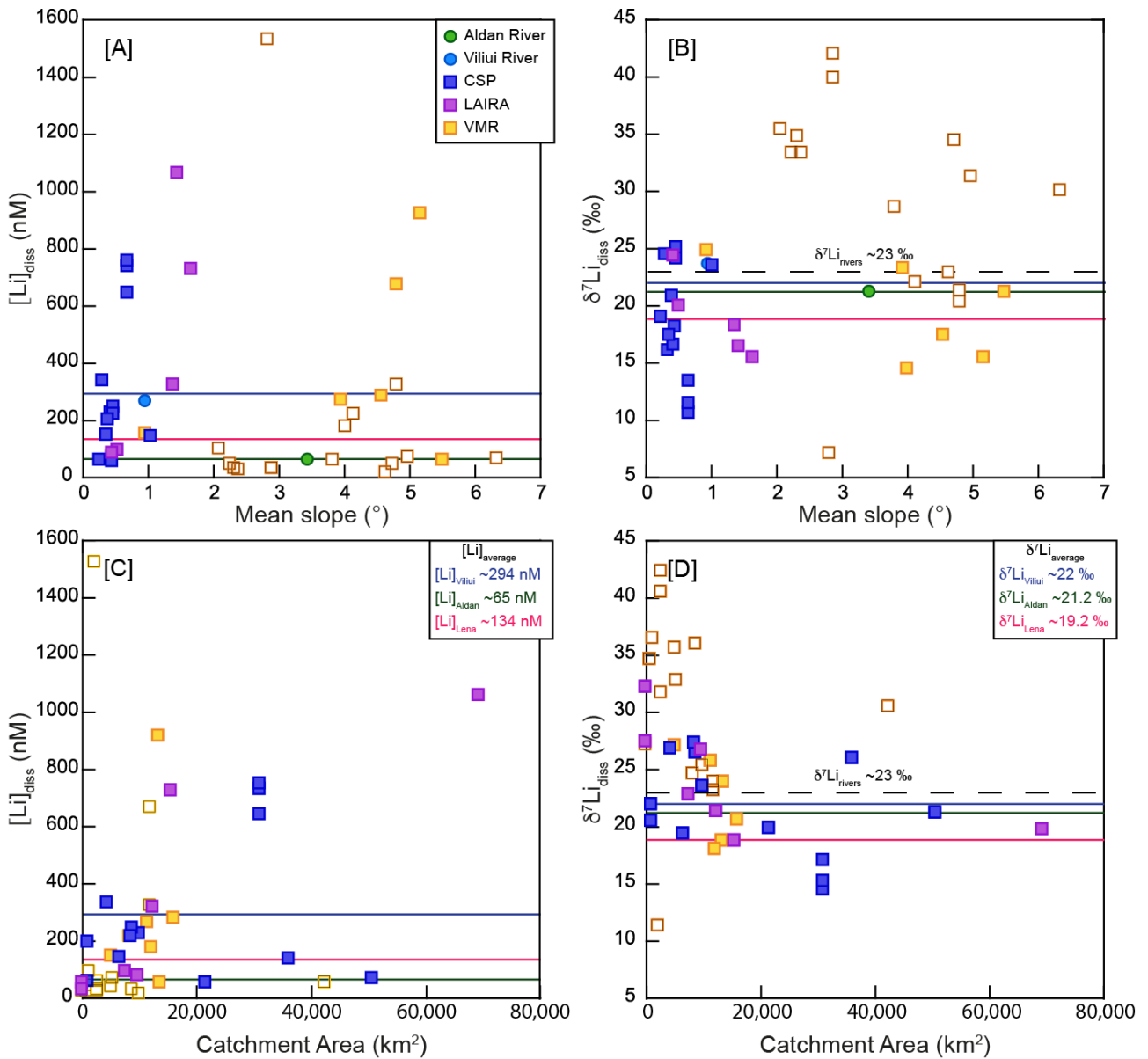


893

894 Figure 2:  $\delta^7\text{Li}_{\text{diss}}$  compositions and dissolved Li concentrations for rivers in the Lena River  
 895 watershed, with previous values from the watershed (Huh et al., 1998a) shown for comparison  
 896 (not shown is one anomalous sample UL436 that drains the evaporitic marine carbonates within  
 897 the Siberian Platform with high [Li] of 3350 nM and  $\delta^7\text{Li}_{\text{diss}} = 21.2\text{‰}$ ). Uncertainties on  $\delta^7\text{Li}$  smaller  
 898 than the symbols. CSP = Central Siberian Plateau; LAIRA = Lena-Amginsky inter-river area; VMR =  
 899 Verkhoyansk Mountain Range. Open symbols represent VMR rivers draining south-facing  
 900 catchments, which show the greatest variation in both [Li] and  $\delta^7\text{Li}_{\text{diss}}$ .

901

902



903

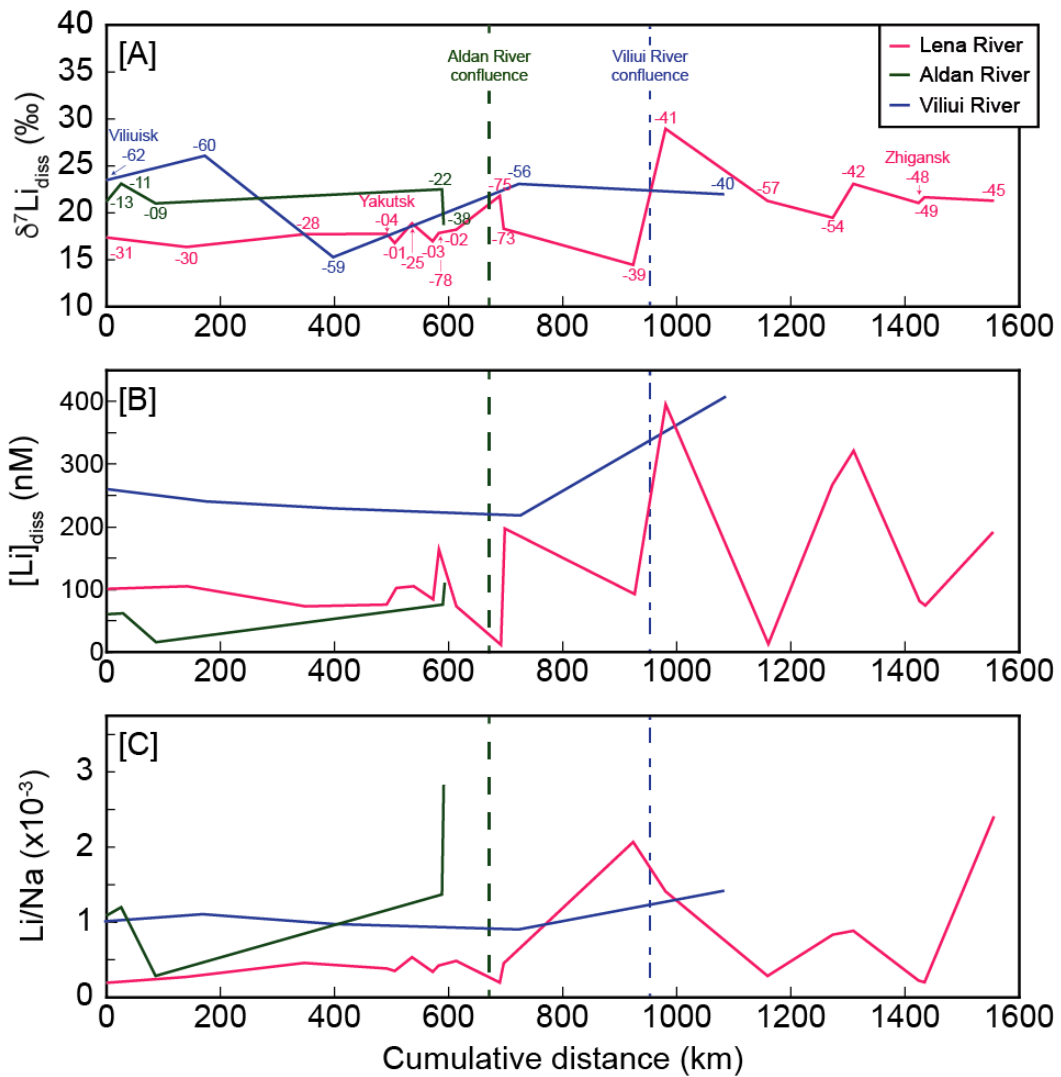
904 Figure 3: Dissolved Li concentrations and  $\delta^{7}\text{Li}$  compositions compared with watershed gradient

905 [A,B] and catchment area [C,D] for tributaries draining into the Lena, Viliui and Aldan Rivers. CSP =

906 Central Siberian Plateau; LAIRA = Lena-Amginsky inter-river area; VMR = Verkhoyansk Mountain

907 Range.

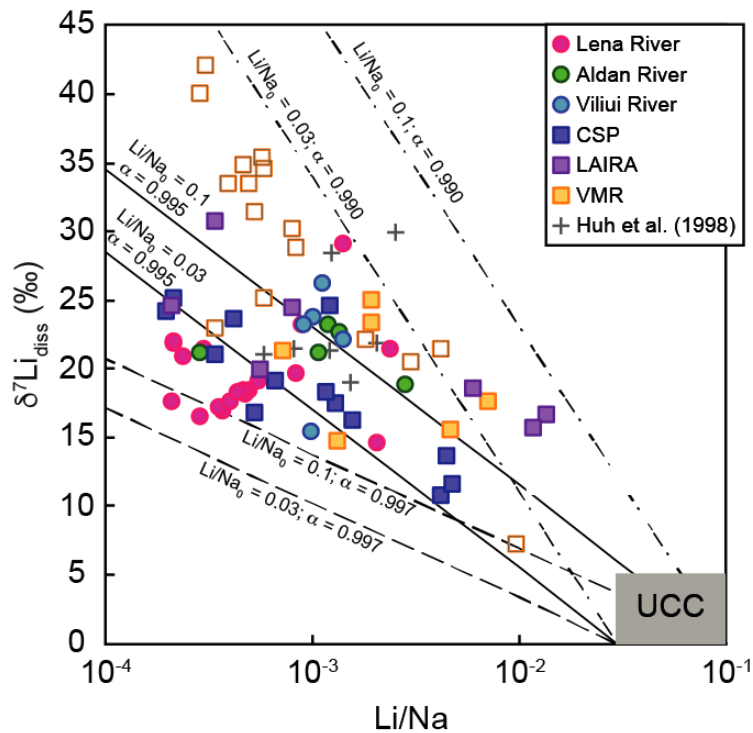
908



909

910 Figure 4: Downstream variations in  $\delta^7\text{Li}_{\text{diss}}$ ,  $[\text{Li}]$  and  $\text{Li}/\text{Na}$  in the Lena River main channel, and  
 911 major tributaries of the Aldan and Viliui Rivers that converge into the main channel. River samples  
 912 numbers are shown adjacent to curves, and arrows indicate the downstream river location of  
 913 major towns. Confluences of the Aldan and Viliui Rivers into the Lena River main channel are  
 914 shown as dashed lines. See Figure 1 for more information. No systematic trends can be observed  
 915 in  $[\text{Li}]$ , or  $\text{Li}/\text{Na}$ . A gradual  $\sim 5\%$  increase can be seen along the Lena River main channel, see text  
 916 for further details.

917

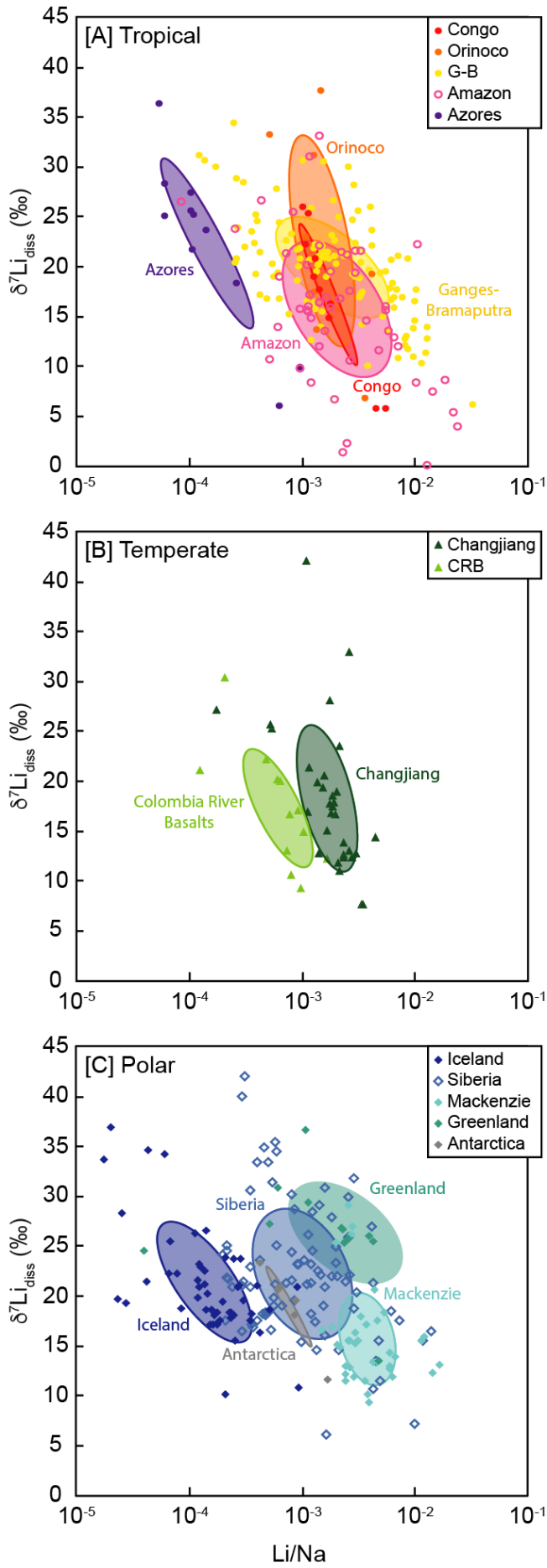


918

919 Figure 5: Relationship between measured  $\delta^7\text{Li}_{\text{diss}}$  and Li/Na molar ratios for the Lena River. Shown  
 920 for comparison are Lena River data from Huh et al. (1998). The lines represent the evolution of  
 921  $\delta^7\text{Li}$  and Li/Na for a model in which Li is supplied to waters by dissolution of primary silicate  
 922 minerals and this is followed by progressive removal of Li into secondary minerals. Curves are  
 923 shown for different starting values and different fractionation factors for Li removal. The grey field  
 924 represents the range of values that are generally expected for dissolution of silicate rocks, with  
 925 Li/Na molar ratios between the highest measured in the Lena River watershed and the  
 926 composition of UCC and  $\delta^7\text{Li}$  values for the upper continental crust and typical shales (Taylor and  
 927 McLennan, 1995; Teng et al., 2004; Dellinger et al., 2014; Sauzéat et al., 2015). CSP = Central  
 928 Siberian Plateau; LAIRA = Lena-Amginsky inter-river area; VMR = Verkhoyansk Mountain Range.  
 929 Open symbols represent VMR rivers draining south-facing catchments.

930





932 Figure 6: A compilation of dissolved Li isotope values versus molar Li/Na for rivers in [A] tropical,  
933 [B] temperate and [C] polar regions. Data include the Lena River and other Siberian rivers (this  
934 study; Huh et al., 1998a); the Mackenzie River (Millot et al., 2003; Millot et al., 2010); Antarctic  
935 rivers (Witherow et al., 2010); Greenland (Wimpenny et al., 2010b); the High Himalayas (Huh et  
936 al., 1998a; Kısakúrek et al., 2005); the Ganges-Brahmaputra (Huh et al., 1998a; Kısakúrek et al.,  
937 2005; Bagard et al., 2015; Frings et al., 2015; Manaka et al., 2017; Pogge von Strandmann et al.,  
938 2017); the Amazon (Huh et al., 1998a; Dellinger et al., 2015); the Orinoco (Stallard et al.,  
939 1995;1996; Huh et al., 1998a); the Congo (Henchiri et al., 2016); Changjiang (Yangtze) River (Huh  
940 et al., 1998a; Liu et al., 2011; Wang et al., 2015); and basalts from Iceland, the Azores and the  
941 Columbia River Basalts (Pogge von Strandmann et al., 2006; Vigier et al., 2009; Pogge von  
942 Strandmann et al., 2010; Liu et al., 2015).

943

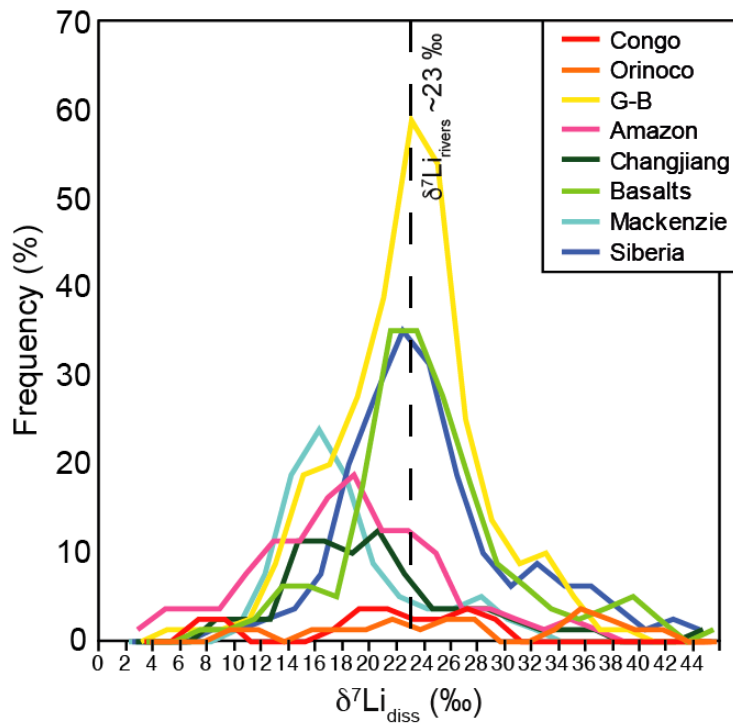
944

945

946

947

948



949

950 Figure 7: Histograms summarising dissolved  $\delta^7\text{Li}$  compositions from large global rivers, and rivers  
 951 draining basaltic terrains. A large peak can be seen clustering around the global median value of  
 952 23‰ (Huh et al., 1998b), with a smaller peak around ~14 to 16‰. Data from same sources as Fig.  
 953 6.